Journal of Medicinal Chemistry

ARTICLE

pubs.acs.org/jmc

Organometallic Half-Sandwich Iridium Anticancer Complexes

Zhe Liu,[†] Abraha Habtemariam,[†] Ana M. Pizarro,[†] Sally A. Fletcher,[†] Anna Kisova,[‡] Oldrich Vrana,[‡] Luca Salassa,[†] Pieter C. A. Bruijnincx,[†,§] Guy J. Clarkson,[†] Viktor Brabec,[‡] and Peter J. Sadler*[,†]

[†]Department of Chemistry, University of Warwick, Gibbet Hill Road, Coventry CV4 7AL, United Kingdom

[‡]Institute of Biophysics, Academy of Sciences of the Czech Republic, v.v.i., Kralovopolska 135, CZ-61265 Brno, Czech Republic

Supporting Information

ABSTRACT: The low-spin $5d^6$ Ir^{III} organometallic half-sandwich complexes $[(\eta^5\text{-}Cp^x)Ir(XY)Cl]^{0/+}$, Cp^x = Cp*, tetramethyl(phenyl)cyclopentadienyl (Cp^{xph}), or tetramethyl(biphenyl)-cyclopentadienyl (Cp^{xbiph}), XY = 1,10-phenanthroline (**4**−**6**), 2,2′-bipyridine (**7**−**9**), ethylenediamine (**10** and **11**), or picolinate (**12**−**14**), hydrolyze rapidly. Complexes with N,N-chelating ligands readily form adducts with 9-ethylguanine but not 9-ethyladenine; picolinate complexes bind to both purines. Cytotoxic potency toward A2780 human ovarian cancer cells increases with phenyl substitution on Cp*: Cp^{xbiph} > Cp^{xph} > Cp*; Cp^{xbiph} complexes **6** and **9** have submicromolar activity. Guanine residues are preferential binding sites for **4**−**6** on plasmid DNA. Hydrophobicity (log *P*), cell and nucleus accumulation of Ir correlate with cytotoxicity, **6** > **5** > **4**; they distribute similarly within cells. The ability to displace DNA intercalator ethidium bromide from DNA correlates with cytotoxicity and viscosity of Ir−DNA adducts. The hydrophobicity and intercalative ability of Cp^{xph} and Cp^{xbiph} make a major contribution to the anticancer potency of their Ir^{III} complexes.

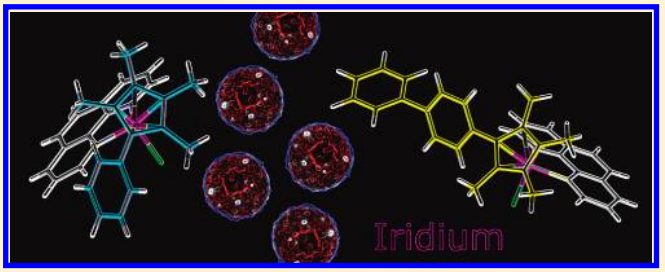

INTRODUCTION

The clinical success of cisplatin, carboplatin, and oxaliplatin[1] has stimulated the search for other transition metal complexes that possess anticancer activity. New metal-based anticancer drugs may be able to widen the spectrum of treatable cancers, reduce toxic side effects, and overcome platinum resistance. Interest in bio-organometallic chemistry and the design of organometallic complexes as anticancer agents is currently increasing.[2] Carbon-bound π-bonded arenes and cyclopentadienyl ligands can provide control of the hydrophilicity and hydrophobicity of the faces of the coordination complex (which influences cell uptake and targeting).[3] Most metallodrugs are prodrugs, and control over ligand substitution is vital if the complex is to reach and react with its target site. In this respect, octahedral low-spin d^6 complexes are attractive for drug design since they are often kinetically inert. Inertness increases from the first to second to third row of transition metals.[4] The lifetime for exchange of an aqua ligand on $[Ir(H_2O)_6]^{3+}$, for example, is about 300 years![5] There are only a limited number of reported studies on the biological activity of iridium complexes. Early studies were concerned with nonorganometallic Ir^I and Ir^{III} complexes,[6] and more recently, a few studies of organometallic Ir^{III} complexes have been reported.[7] Iridium(III) complexes are generally thought to be too inert to possess high reactivity. Indeed, the inertness of Ir^{III} has allowed the design of complexes that function as rigid scaffolds and inhibit kinase enzymes, for example.[8] The biological inactivity of *trans*-$[IrCl_4(DMSO)(Im)][ImH]$[9] and *trans*-$[IrCl_4(Im)_2][ImH]$ (ImH = imidazole),[10] Ir^{III} analogues of the Ru^{III} anticancer drugs NAMI-A and the imidazole analogue of the indazole complex KP1019, respectively, has been attributed to the kinetic inertness of Ir^{III}.

Organometallic Ru^{II} and Os^{II} arene anticancer complexes of the type $[(\eta^6\text{-arene})(Ru/Os)(NN)Cl]^+$, where NN is a chelating diamine ligand, can be activated by hydrolysis of the Ru/Os−Cl bond, prior to binding to DNA.[11] The arene is important in determining the anticancer activity and nature of the DNA distortions. In particular, when the arene has an extended ring system(e.g., biphenyl or tetrahydroanthracene), direct binding to DNA bases (largely guanine) can be accompanied by arene intercalation between the bases.[12]

Neutral arene ligands do not stabilize Ir^{III}. In contrast, negatively charged pentamethylcyclopentadienyl (Cp*) is an excellent stabilizing ligand for Ir^{III}. In the work reported here, we apply the design concepts discovered for Ru^{II} and Os^{II} arene complexes to Ir^{III} Cp* and functionalized Cp* complexes $[(\eta^5\text{-}Cp^x)Ir(XY)Cl]^{0/+}$ containing N,N-bound 1,10-phenanthroline (phen), 2,2′-bipyridine (bpy), ethylenediamine (en), and N,O-bound picolinate (pico) as chelating ligands. Iridium(III) Cp* complexes have attracted recent attention as catalysts, for example, in hydrogen transfer reactions.[13] Only a few iridium complexes containing functionalized Cp* ligands have been reported previously.[14] We have studied the effect of Cp* functionalization on the rate of hydrolysis, acidity of the aqua adducts, interactions with nucleobases, hydrophobicity (octanol/water partition), cell accumulation (the net effect of uptake and efflux)

Received: January 27, 2011
Published: March 28, 2011

Chart 1. Iridium Cyclopentadienyl Complexes Studied in This Work

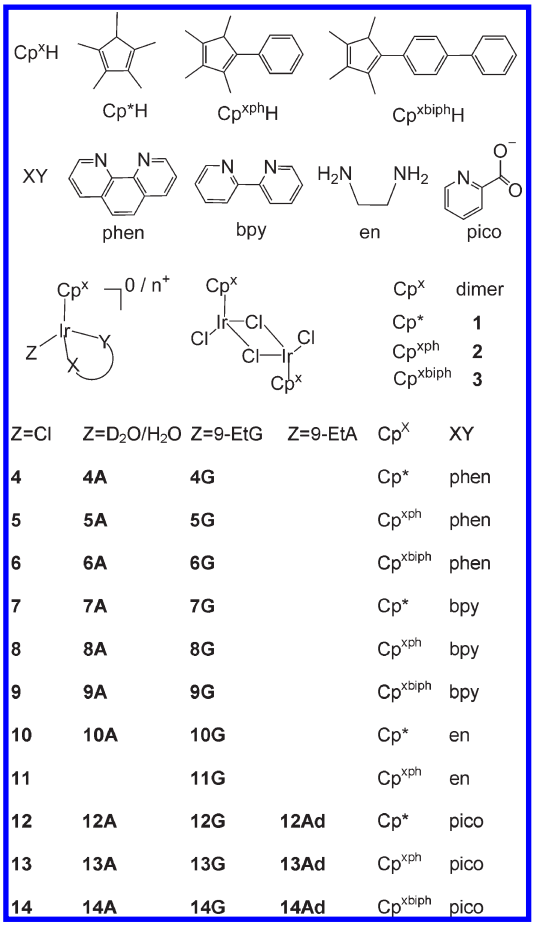

Z=Cl	Z=D_2O/H_2O	Z=9-EtG	Z=9-EtA	Cp^X	XY
4	**4A**	**4G**		Cp*	phen
5	**5A**	**5G**		Cp^{xph}	phen
6	**6A**	**6G**		Cp^{xbiph}	phen
7	**7A**	**7G**		Cp*	bpy
8	**8A**	**8G**		Cp^{xph}	bpy
9	**9A**	**9G**		Cp^{xbiph}	bpy
10	**10A**	**10G**		Cp*	en
11		**11G**		Cp^{xph}	en
12	**12A**	**12G**	**12Ad**	Cp*	pico
13	**13A**	**13G**	**13Ad**	Cp^{xph}	pico
14	**14A**	**14G**	**14Ad**	Cp^{xbiph}	pico

and distribution, interaction with DNA, and cytotoxicity to cancer cells.[15] We show that such complexes can be thermodynamically stable and yet kinetically labile toward substitution reactions and that substituents on the cyclopentadienyl ring and chelating ligand can have a dramatic effect on chemical and biological activity. This appears to be the first time that tetramethyl(phenyl)cyclopentadienyl (Cp^{xph}) and tetramethyl(biphenyl)cyclopentadienyl (Cp^{xbiph}) have been used as ligands in iridium complexes.

RESULTS

Chemistry. *Syntheses.* Eleven Ir^{III} half-sandwich complexes (Chart 1) of the type $[(\eta^5\text{-}Cp^x)Ir(XY)Cl]^{0/+}$, where Cp^x is Cp* or its phenyl Cp^{xph} or biphenyl Cp^{xbiph} derivatives and XY is the N,N-chelating ligand 1,10-phenanthroline (phen, **4**−**6**), 2,2′-bipyridine (bpy, **7**−**9**), ethylenediamine[16] (en, **10** and **11**), or N,O-chelating picolinate (pico, **12**−**14**), were synthesized and characterized, and their cancer cell cytotoxicity was investigated. Their structures were studied by X-ray crystallography and by density functional theory (DFT) calculations, and their aqueous solution chemistry by hydrolysis measurements, pK_a determination for aqua adducts, and interactions with nucleobases guanine and adenine. To elucidate the pronounced effect of the Cp^x ligand on biological activity, detailed comparisons were made between the three phen complexes **4**−**6** involving partition coefficients, distribution in cancer cells, DNA replication mapping, ethidium bromide displacement from DNA, and effect on DNA viscosity.

Complexes **4**−**14** were synthesized in moderate yields by reaction of 1,10-phenanthroline, 2,2′-bipyridine, ethylenediamine, or 2-picolinate, with the appropriate dimer $[(\eta^5\text{-}Cp^x)IrCl_2]_2$ in methanol. The derivative $Cp^{xbiph}H$, in which one of the ring methyls of Cp* is replaced by a biphenyl group, has not been previously reported. All of the synthesized complexes were fully characterized by ^1H NMR spectroscopy and CHN elemental analysis. Introduction of phenyl substituents on the Cp* ring decreased the reaction yields significantly. Complexes **4** and **7** were isolated as Cl^- salts, complex **11** as a BPh_4^- salt, and complexes **5**, **6**, and **8**−**10** as PF_6^- salts. The complexes studied in this work are shown in Chart 1.

X-ray Crystal Structures and Computation. The X-ray crystal structures of $[(\eta^5\text{-}C_5Me_4C_6H_5)IrCl_2]_2$ (**2**), $[(\eta^5\text{-}C_5Me_4C_6H_5)Ir(phen)Cl]PF_6$ (**5**·PF_6), $[(\eta^5\text{-}C_5Me_4C_6H_5)Ir(bpy)Cl]PF_6$ (**8**·PF_6), $[(\eta^5\text{-}C_5Me_4C_6H_4C_6H_5)Ir(bpy)Cl]PF_6$ (**9**·PF_6), $[(\eta^5\text{-}C_5Me_4C_6H_5)Ir(en)Cl]BPh_4$ (**11**·BPh_4), and $[(\eta^5\text{-}C_5Me_4C_6H_5)Ir(pico)Cl]$ (**13**) were determined. The complexes adopt the expected half-sandwich pseudo-octahedral "three-leg piano-stool" geometry with the iridium bound to an η^5-cyclopentadienyl ligand (Ir to ring centroid 1.747−1.789 Å), a chloride (2.384−2.415 Å), and a chelating ligand. Their structures and atom numbering schemes are shown in Figure 1 and Figure S1 in the Supporting Information. Crystallographic data are shown in Table S1 in the Supporting Information, and selected bond lengths and angles are listed in Table S2 in the Supporting Information.

In the structure of the Cp^{xph} dimer **2**, one of the chlorides (Cl1 or Cl2) acts as a bridging ligand to a symmetry-related molecule across an inversion center. The Ir−Ir bond distance is 3.7157(4) Å, and the angle between mean planes through the phenyl and the cyclopentadienyl groups is 68.21°. The phenyl group is involved in a weak $\pi-\pi$ interaction with a symmetry-related phenyl group of a neighboring ligand in the unit cell (Figure S2 in the Supporting Information). The two interacting π systems are parallel, with a centroid−centroid distance of 3.956 Å. Further intermolecular ring stacking is observed in the crystal structures of complex **5**·PF_6, between phen ligands in neighboring molecules (3.518 Å) (Figure S3 in the Supporting Information).

The structures of the Ir^{III} complexes **5**·PF_6, **8**·PF_6, and **9**·PF_6 containing chelated phen or bpy are shown in Figure 1. The Ir−Cl and Ir−N bond lengths range from 2.3840(14) to 2.3891(5) Å and from 2.083(6) to 2.1001(17) Å, respectively (Table S2 in the Supporting Information). Stacking between the Cp^{xbiph} ligands of neighboring molecules is present in crystals of complex **9**·PF_6. The centroids of the three rings on independent molecules are separated by 4.447, 4.607, and 4.447 Å, at dihedral angles of 8.47, 0, and 8.47°, respectively (Figure S4 in the Supporting Information). The twist angle between the cyclopentadienyl and the central ring is 45.23°, and between the central and the terminal phenyl ring, it is 46.34°. In contrast, the planes of the terminal and bound rings are only twisted by 8.47°.

The propeller twist of the phenyl-tetramethylcyclopentadienyl ligand in complex **11**·BPh_4 is 63.7°. The Ir−Cl bond length [2.4152(12) Å] is the longest of these five X-ray structures.

The geometries of complexes **4**−**14** were optimized using the PBE0 functional (Table S3 in the Supporting Information; the description of frontier orbitals is in the Supporting Information). Selected calculated bond lengths are listed in Table S4 in the Supporting Information and are in good agreement with the

dx.doi.org/10.1021/jm2000932 |J. Med. Chem. 2011, 54, 3011–3026

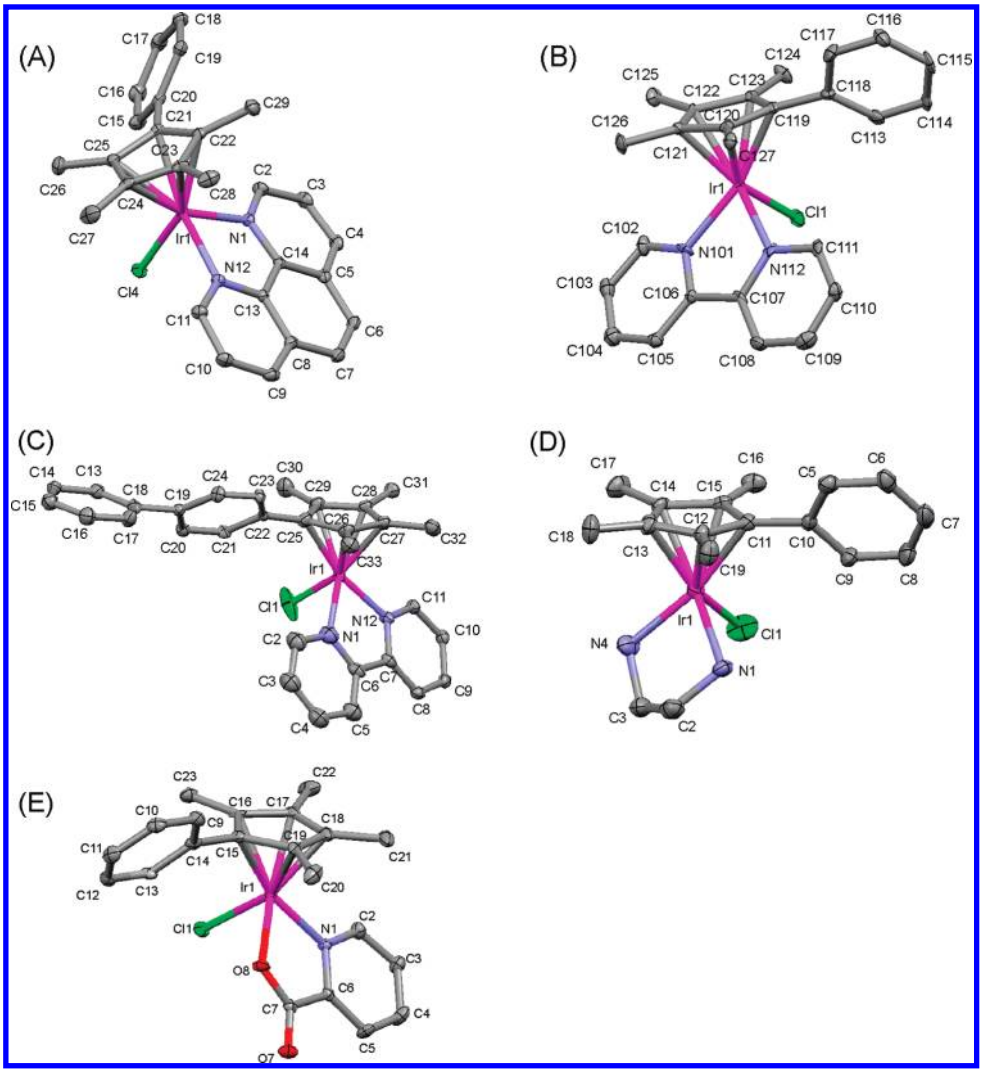

Figure 1. X-ray crystal structures with atom numbering schemes for (A) $[(\eta^5\text{-}C_5Me_4C_6H_5)Ir(phen)Cl]PF_6$ (**5**·PF_6), (B) $[(\eta^5\text{-}C_5Me_4C_6H_5)Ir(bpy)Cl]PF_6$ (**8**·PF_6), (C) $[(\eta^5\text{-}C_5Me_4C_6H_4C_6H_5)Ir(bpy)Cl]PF_6$ (**9**·PF_6), (D) $[(\eta^5\text{-}C_5Me_4C_6H_5)Ir(en)Cl]BPh_4$ (**11**·BPh_4), and (E) $[(\eta^5\text{-}C_5Me_4C_6H_5)Ir(pico)Cl]$ (**13**), with thermal ellipsoids drawn at 50% probability. The hydrogen atoms and counterions have been omitted for clarity.

experimental X-ray structures in the case of **5**·PF_6, **8**·PF_6, **9**·PF_6, and **11**·BPh_4. DFT calculations show that Ir−Cl and Ir−cyclopentadienyl ring bond distances remain similar on changing Cp* to substituted Cp* groups.

Electrostatic potential surfaces (EPSs) for phen chlorido complexes **4**−**6** and aqua adduct **6A** and the pico chlorido complexes **12**−**14** and aqua adduct **14A** were calculated. N,N-chelating phen complexes **4**−**6** show more positive electrostatic potentials than the N,O-chelating pico complexes **12**−**14** (Figure 2). Moreover, a higher electron density is present on the second phenyl ring of the Cp^{xbiph} ligand in complexes **6** and **14**. The same trend is observed in the EPSs of the aqua derivatives $[(\eta^5\text{-}C_5Me_4C_6H_4C_6H_5)Ir(phen)(H_2O)]^{2+}$ (**6A**) and $[(\eta^5\text{-}C_5Me_4C_6H_4C_6H_5)Ir(pico)(H_2O)]^{+}$ (**14A**), which as expected show more positive surfaces as compared to their chlorido analogues, **6** and **14**.

Hydrolysis Studies. Hydrolysis of M−Cl bonds can represent an activation step for transition metal anticancer complexes.[17] $M-OH_2$ aqua complexes are often more reactive than the relevant chlorido complexes.[18] The hydrolysis of compounds **4**−**10** and **12**−**14** in 5% MeOD-d_4/95% D_2O (v/v) was monitored by ^1H NMR at different temperatures from 278 to 293 K. The presence of methanol ensured the solubility of the complexes.

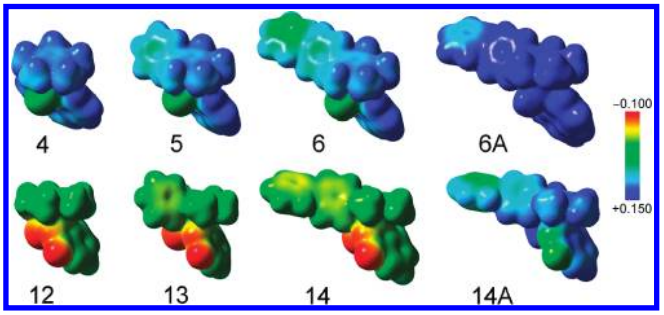

Figure 2. EPSs of the phen chlorido complexes **4**−**6** and aqua adduct **6A** and the pico chlorido complexes **12**−**14** and aqua adduct **14A**. EPS surfaces are shown in both space (with positive and negative regions in blue and red, respectively) and mapped on electron density (isovalue 0.004) of the molecules. The electrostatic potential is represented with a color scale going from red (−0.100 au) to blue (0.150 au).

dx.doi.org/10.1021/jm2000932 |*J. Med. Chem.* 2011, 54, 3011–3026

Table 1. Hydrolysis Data for Complexes 4−10 and 12−14 at Various Temperatures

	k (min^{-1}) $t_{1/2}$ (min)					
complex[a]	278 K	283 K	288 K	293 K	310 K[e]	K_{aq} (mM)[b]
4	*c*					0.04
5	0.027	0.047	0.083	*d*	0.65	0.06
	25.4	14.6	8.3	*d*	1.1	
6	0.022	*d*	0.044	0.065	0.18	0.29
	31.8	*d*	15.9	10.7	3.8	
7	*c*					0.05
8	0.031	0.062	0.099	*d*	0.89	0.08
	22.1	11.1	7.0	*d*	0.8	
9	0.026	0.041	*d*	0.078	0.23	1.45
	26.7	16.9	*d*	8.8	3.0	
10	*c*					0.44
12	*c*					0.78
13	*c*					1.11
14	*c*					2.33

[a] The course of the hydrolysis of complex **11** was difficult to interpret from NMR spectra. [b] 278 K. [c] Too fast to be measured. [d] Not determined. [e] Obtained from the Arrhenius equation.

All of these Ir^{III} complexes undergo relatively rapid hydrolysis. Complexes $[(\eta^5\text{-}C_5Me_5)Ir(phen)Cl]^+$ (**4**), $[(\eta^5\text{-}C_5Me_5)Ir(bpy)Cl]^+$ (**7**), and $[(\eta^5\text{-}C_5Me_5)Ir(en)Cl]^+$ (**10**) containing Cp* and $[(\eta^5\text{-}C_5Me_5)Ir(pico)Cl]$ (**12**), $[(\eta^5\text{-}C_5Me_4C_6H_5)Ir(pico)Cl]$ (**13**), and $[(\eta^5\text{-}C_5Me_4C_6H_4C_6H_5)Ir(pico)Cl]$ (**14**) containing picolinate hydrolyzed too rapidly for the rates to be determined by ^{1}H NMR spectroscopy even at 278 K: there was little change in the spectra between 5 min and 24 h, Figure S5 in the Supporting Information. Attempts to observe hydrolysis of these complexes by UV−vis at 288 K were also unsuccessful: Equilibrium was reached before the first UV−vis spectrum was acquired (<1 min), Figure S6 in the Supporting Information.

To confirm the hydrolysis of these complexes, NaCl (1−4 mol equiv) was added to equilibrium solutions. With an increase in the NaCl concentration, ^{1}H NMR peaks for the chlorido adducts increased while peaks for the aqua form decreased in intensity (Figures S7−S9 in the Supporting Information). Similarly, the addition of NaCl to an aqueous solution of the aqua complex **4A** gave rise to peaks for the chlorido complex **4** (Figure S10 in the Supporting Information).

The hydrolysis of complexes $[(\eta^5\text{-}C_5Me_4C_6H_5)Ir(phen)Cl]^+$ (**5**), $[(\eta^5\text{-}C_5Me_4C_6H_4C_6H_5)Ir(phen)Cl]^+$ (**6**), $[(\eta^5\text{-}C_5Me_4C_6H_5)Ir(bpy)Cl]^+$ (**8**), and $[(\eta^5\text{-}C_5Me_4C_6H_4C_6H_5)Ir(bpy)Cl]^+$ (**9**) was slow enough to be studied by ^{1}H NMR at low temperature. Hydrolysis was monitored at temperatures ranging from 278 to 293 K by observing the appearance of new ^{1}H NMR peaks over time. The time dependence for formation of the aqua adducts of **5**, **6**, **8**, and **9** was fitted to pseudo first-order kinetics (Figure S11 in the Supporting Information), and their hydrolysis rate constants, half-lives, and extent of hydrolysis were determined (Table 1). At 278 K, the half-life for hydrolysis of the biphenyl-substituted Cp^{xbiph} complex **6** was 32 min, about 1.3 times slower than that of the phenyl-Cp* complex **5** (25 min; Table 1). The half-lives and extent of hydrolysis of complexes **4**−**6** at 278 K increase with the size of the ring system in the order $Cp^{xbiph} > Cp^{xph} > Cp^*$. This trend is also observed for complexes **7**−**9**.

Table 2. pK_a^* and pK_a Values[a] for the Deprotonation of the Coordinated D_2O in Complexes 4A−10A and 12A−14A

aqua complex	pK_a^*	pK_a
$[(\eta^5\text{-}C_5Me_5)Ir(phen)(D_2O)]^{2+}$ (**4A**)	7.88	7.74
$[(\eta^5\text{-}C_5Me_4C_6H_5)Ir(phen)(D_2O)]^{2+}$ (**5A**)	7.68	7.55
$[(\eta^5\text{-}C_5Me_4C_6H_4C_6H_5)Ir(phen)(D_2O)]^{2+}$ (**6A**)	7.50	7.38
$[(\eta^5\text{-}C_5Me_5)Ir(bpy)(D_2O)]^{2+}$ (**7A**)	6.94	6.86
$[(\eta^5\text{-}C_5Me_4C_6H_5)Ir(bpy)(D_2O)]^{2+}$ (**8A**)	6.31	6.28
$[(\eta^5\text{-}C_5Me_4C_6H_4C_6H_5)Ir(bpy)(D_2O)]^{2+}$ (**9A**)	6.68	6.63
$[(\eta^5\text{-}C_5Me_5)Ir(en)(D_2O)]^{2+}$ (**10A**)	7.66	7.54
$[(\eta^5\text{-}C_5Me_5)Ir(pico)(D_2O)]^{+}$ (**12A**)	8.15	7.99
$[(\eta^5\text{-}C_5Me_4C_6H_5)Ir(pico)(D_2O)]^{+}$ (**13A**)	7.75	7.62
$[(\eta^5\text{-}C_5Me_4C_6H_4C_6H_5)Ir(pico)(D_2O)]^{+}$ (**14A**)	7.65	7.52

[a] pK_a values were calculated from pK_a^* according to Krezel and Bal.[20]

The hydrolysis rate constants and half-lives of **5**, **6**, **8**, and **9** at 310 K (body temperature) were calculated using the Arrhenius equation and are listed in Table 1. These range from 1 min for complexes **5** and **8** to 4 min for complex **6**. In each series of complexes containing different chelating N,N- or N,O-ligands, the equilibrium constants (K_{aq}) for hydrolysis at 278 K increase with increasing phenyl substitution on the Cp^x ligand (Table 1).

The effect of added chloride on the aqueous chemistry of **7** was investigated. ^{1}H NMR spectra of 1 mM **7** in 104, 23, or 4 mM NaCl in D_2O (mimicking the chloride concentrations in blood plasma, cell cytoplasm, and cell nucleus, respectively)[18b,19] were recorded within 10 min of sample preparation and after incubation at 310 K for 24 h. On the basis of ^{1}H NMR peak integrals, almost no hydrolyzed complex **7** (**7A**) was found to be present in 104 mM [Cl] or in 23 mM [Cl], and only 5% of aqua complex **7A** was observed at 4 mM [Cl] after 10 min with no further change after 24 h.

pK_a^* Determination. The pK_a of coordinated water can have a significant influence on its reactivity since M−OH bonds are often much less labile than $M-OH_2$ bonds;[11b] moreover, hydroxide is a good bridging ligand and can give rise to oligomeric species. Changes in the ^{1}H NMR chemical shifts for coordinated chelating ligands in aqua complexes **4A**−**9A**, **12A**−**14A**, and methyl groups of Cp* in aqua complex **10A** were followed with a change in pH* over a range of 2−11 (Figure S12 in the Supporting Information). ^{1}H NMR peaks assigned to aqua complexes gradually shifted to high field with increase in pH*. The resulting pH titration curves were fitted to the Henderson−Hasselbalch equation, from which the pK_a^* values of the coordinated water were determined. This gave rise to pK_a values between 6.28 and 7.99 (Table 2), with the bpy complexes being the most acidic (pK_a values 6.28−6.86) and the pico complexes the least acidic (pK_a values 7.52−7.99).

Interactions with Nucleobases. Because DNA is a potential target site for transition metal anticancer complexes,[21] the binding of 9-ethylguanine (9-EtG) and 9-ethyladenine (9-EtA) to complexes **4**−**14**, and aqua complex **5A** was studied. The extent of nucleobase adduct formation by these complexes based on ^{1}H NMR peak integrals is shown in Table 3.

The addition of 1 mol equiv of 9-EtG to an equilibrium solution of complex **5**, $[(\eta^5\text{-}C_5Me_4C_6H_5)Ir(phen)Cl]^+$ (1.0 mM), in 5% MeOD-d_4/95% D_2O (v/v, pH* 7.2) at 310 K resulted in 15% of **5** reacting after 10 min and a new 9-EtG H8 peak appearing at 7.68 ppm (species **5G**, Figure S13 in the Supporting Information),

dx.doi.org/10.1021/jm2000932 |J. Med. Chem. 2011, 54, 3011–3026

Table 3. Extent of 9-EtG and 9-EtA Adduct Formation for Complexes 4−14 and 5A (ca. 1 mM) at 310 K after 24 h

	Cp^x	XY	G adduct (%)	A adduct (%)
4	Cp^*	phen(N,N−)	83	0
5	Cp^{xph}	phen(N,N−)	42	0
5A	Cp^{xph}	phen(N,N−)	74	0
6	Cp^{xbiph}	phen(N,N−)	90	0
7	Cp^*	bpy(N,N−)	61	0
8	Cp^{xph}	bpy(N,N−)	47	0
9	Cp^{xbiph}	bpy(N,N−)	65	0
10	Cp^*	en(N,N−)	100	0
11	Cp^{xph}	en(N,N−)	100	0
12	Cp^*	pico(N,O−)	100	81
13	Cp^{xph}	pico(N,O−)	100	76
14	Cp^{xbiph}	pico(N,O−)	100	71

shifted by 0.15 ppm to high field relative to that of free 9-EtG. After 24 h, 42% of **5** had reacted. The ESI-MS of an equilibrium solution (Figure S14 in the Supporting Information) contained a major peak at m/z 374.6, confirming the formation of the 9-EtG adduct **5G**, $[(\eta^5\text{-}C_5Me_4C_6H_5)Ir(phen)(9\text{-}EtG)]^{2+}$ (calcd m/z 374.5). However, 65% of aqua complex **5A** (prepared by treating a solution of **5** with 1 mol equiv of $AgNO_3$) reacted with 9-EtG to form **5G** after 10 min and 73% after 24 h. More than 80% of complexes **4** and **6** reacted with 9-EtG under the same conditions.

Complexes $[(\eta^5\text{-}C_5Me_5)Ir(en)Cl]^+$ (**10**) and $[(\eta^5\text{-}C_5Me_4C_6H_5)Ir(en)Cl]^+$ (**11**) interestingly showed an exceptionally high affinity for 9-EtG with 100% nucleobase adduct formation within 10 min. On addition of a solution of 1 mol equiv of 9-EtG gradually to an equilibrium solution of **10** (0.9 mM) in 5% MeOD-d_4/95% D_2O (v/v) at 310 K, Figure S15 in the Supporting Information, the methyl peak for **10** and **10A** decreased in intensity and eventually disappeared. A new Cp^* methyl peak (for **10G**) appeared at 1.65 ppm. When 9-EtG was in excess, a set of new peaks assignable to free 9-EtG was clearly visible (Figure S15 in the Supporting Information).

The geometry of the adduct (**7G**) between complex **7** and 9-EtG was optimized by DFT calculations. These gave an Ir−N7(9-EtG) distance of 2.14 Å. The Ir−N and Ir−cyclopentadienyl ring bond distances increase by 0.1−0.2 Å as compared to complex **7**. The highest occupied molecular orbital (HOMO) of the adduct is 9-EtG-centered and the lowest unoccupied molecular orbital (LUMO) has bpy character (see Table S3 in the Supporting Information).

The addition of 1 mol equiv of 9-EtA to an equilibrium solution of **5** (1.0 mM) in 5% MeOD-d_4/95% D_2O (v/v) at 310 K resulted in no additional ^1H NMR peaks over a period of 24 h (Figure S16 in the Supporting Information). Similarly, no reaction with 9-EtA was observed for other complexes containing N,N-chelating ligands (Table 3).

In contrast, compounds **12**−**14** containing pico as chelating ligand formed both 9-EtG and 9-EtA adducts to the extent of 100% and more than 70% completion, respectively, after 24 h. Two adenine nucleobase adducts are formed in the reaction of complexes **12**−**14** with 9-EtA, most likely through iridium binding to N1 or N7 of adenine forming 9-EtA adducts in 1:3.1, 1:3.2, and 1:3.0 ratios, respectively (Figure S17 in the Supporting Information).

Cancer Cell and DNA Studies. *Cytotoxicity.* The cytotoxicity of complexes **4**−**14** toward A2780 human ovarian cancer cells was investigated; see Table 4. The IC_{50} values (concentration at

Table 4. Inhibition of Growth of A2780 Human Ovarian Cancer Cells by Complexes 4−14 and Comparison with Cisplatin

complex	IC_{50}[a] (μM)
$[(\eta^5\text{-}C_5Me_5)Ir(phen)Cl]Cl$ (**4**·Cl)	>100
$[(\eta^5\text{-}C_5Me_4C_6H_5)Ir(phen)Cl]PF_6$ (**5**·PF_6)	6.70 ± 0.62
$[(\eta^5\text{-}C_5Me_4C_6H_4C_6H_5)Ir(phen)Cl]PF_6$ (**6**·PF_6)	0.72 ± 0.01
$[(\eta^5\text{-}C_5Me_5)Ir(bpy)Cl]Cl$ (**7**·Cl)	>100
$[(\eta^5\text{-}C_5Me_4C_6H_5)Ir(bpy)Cl]PF_6$ (**8**·PF_6)	15.86 ± 1.49
$[(\eta^5\text{-}C_5Me_4C_6H_4C_6H_5)Ir(bpy)Cl]PF_6$ (**9**·PF_6)	0.57 ± 0.09
$[(\eta^5\text{-}C_5Me_5)Ir(en)Cl]PF_6$ (**10**·PF_6)	>100
$[(\eta^5\text{-}C_5Me_4C_6H_5)Ir(en)Cl]BPh_4$ (**11**·BPh_4)	16.97 ± 0.05
$[(\eta^5\text{-}C_5Me_5)Ir(pico)Cl]$ (**12**)	>100
$[(\eta^5\text{-}C_5Me_4C_6H_5)Ir(pico)Cl]$ (**13**)	>100
$[(\eta^5\text{-}C_5Me_4C_6H_4C_6H_5)Ir(pico)Cl]$ (**14**)	16.30 ± 0.32
cisplatin	1.22 ± 0.12

[a] The drug treatment period was 24 h.

Table 5. log *P* Values for Complexes 4−6[a]

	log *P*	
complex	mean	SD
4	−0.82	0.01
5	0.48	0.03
6	1.11	0.17

[a] Results are the means of three independent experiments and are expressed as means ± SDs.

which 50% of the cell growth is inhibited) for Cp^* complexes **4**, **7**, **10**, and **12** and the Cp^{xph} pico complex **13** were all >100 μM and are thus deemed as inactive. However, compounds **5**, **6**, **8**, **9**, **11**, and **14** were all active. Complexes **5**, **8**, and **11** containing Cp^{xph} and **14** containing Cp^{xbiph} showed good activity, displaying IC_{50} values of 6−17 μM.

Complexes **6** and **9** containing Cp^{xbiph} exhibited potent cytotoxicity with IC_{50} values of 0.7 and 0.6 μM, respectively, ca. twice as active as cisplatin in the A2780 cell line (IC_{50} = 1.2 μM). For all four series of complexes containing different chelating N,N- or N,O-ligands, the trend of increasing of activity with increasing phenyl substitution was the same: Cp^{xbiph} > Cp^{xph} > Cp^*.

Hydrophobicity (log P). The octanol/water partition coefficients (log *P*) for the phen complexes **4**−**6** were determined since lipophilicity correlates with cytotoxic potency for some reported series of metallodrugs.[22] The determined values are listed in Table 5. The addition of NaCl (200 mM) was used to suppress hydrolysis of the compounds, ensuring that log *P* values for the chlorido and not aqua complexes were determined. The log *P* values increase in the order **4** < **5** < **6**. Only complex **4**, containing the unsubstituted Cp^* ligand, has a negative log *P* value (partitions preferentially into water, Table 5).

Cell Accumulation and DNA Binding. Because increased lipophilicity has often been linked to increased cell uptake and cytotoxicity,[23] the accumulation and DNA binding of complexes **4**−**6** by A2780 ovarian cancer cells was determined after 24 h of exposure to 5 μM concentrations of the complexes. DNA from A2780 cells was isolated, and the Ir content was determined. The Cp^{xbiph} complex **6** gave rise to the highest level of iridium on

dx.doi.org/10.1021/jm2000932 |J. Med. Chem. 2011, 54, 3011–3026

Table 6. Iridium Accumulation and Binding to DNA in A2780 Human Ovarian Cancer Cells[a]

	cell accumulation (ng Ir/10^6 cells)		DNA binding (ng Ir/10^6 cells)	
complex	mean	SD	mean	SD
4	3.9	0.2	0.3	0.04
5	23.5	3.7	1.3	0.3
6	88.8	20.0	5.3	1.6

[a] The drug treatment period was 24 h with 5 μM Ir^{III} complexes. Each value represents the mean ± SD for two independent experiments done in triplicate.

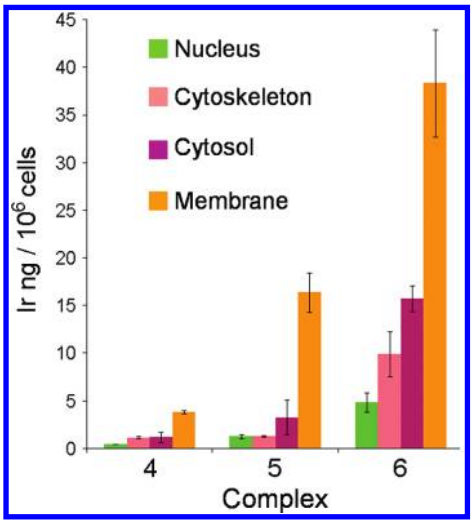

Figure 3. Iridium content of the nucleus, cytosol, membrane, and cytoskeleton fractions (ng Ir/10^6 cells) of A2780 cells after 24 h of exposure to 5 μM **4**–**6**. Results are the means of two independent experiments in triplicate and are expressed as means ± SDs.

DNA, ca. 4× that of complex **5** and 20× that of complex **4** (Table 6). Of the total Ir taken up by the cells, 7.7% for **4**, 5.5% for **5**, and 6.0% for **6** was bound to DNA.

Distribution of Iridium in Cell Fractions. The iridium content of the nucleus, cytosol, membrane, and cytoskeleton fractions isolated from A2780 cells after 24 h of exposure to the phen complexes **4**–**6** was determined, and the results are shown in Table S5 in the Supporting Information and Figure 3. The extent of accumulation of the three complexes into the different cell fractions was similar to that observed for whole cell accumulation: **6** > **5** > **4**. The highest concentration of iridium was in the cell membrane/particulate fraction, accounting for 54 (**6**), 74 (**5**), and 59% (**4**) of the total Ir in the cell. For all complexes, the next highest concentration of Ir was in the cytosol, accounting for 24 (**6**), 15 (**5**), and 17% (**4**).

For the two remaining fractions, the Ir concentration dropped significantly. For complexes **4** and **6**, the cytoskeleton was the next major compartment for Ir accumulation. The amount of Ir in the nucleus was significant and similar for all three Ir^{III} complexes, 7.2% of the total Ir for **6**, 5.8% for **5**, and 6.4% for **4**, and similar in proportion to that bound to DNA.

Replication Mapping of Iridium-DNA Adducts. This procedure involved the extension by VentR(exo-) DNA polymerase of the 3′-end of the primer up to the metal adduct on the template strand of pSP73KB DNA linearized by *Hpa*I restriction endonuclease. The products of the synthesis were then examined on DNA sequencing gels, and the sequence specificity of iridium adduct formation was determined to the exact base pair. In vitro DNA synthesis on DNA templates containing the adducts of the phen complexes **4**–**6** generated a population of DNA fragments, indicating that the adducts of these complexes effectively terminated DNA synthesis (Figure 4A, lanes 4–6). Complexes **4**–**6** exhibit a sequence dependence of the inhibition clearly different from that of cisplatin. The Ir compounds form more blocks on

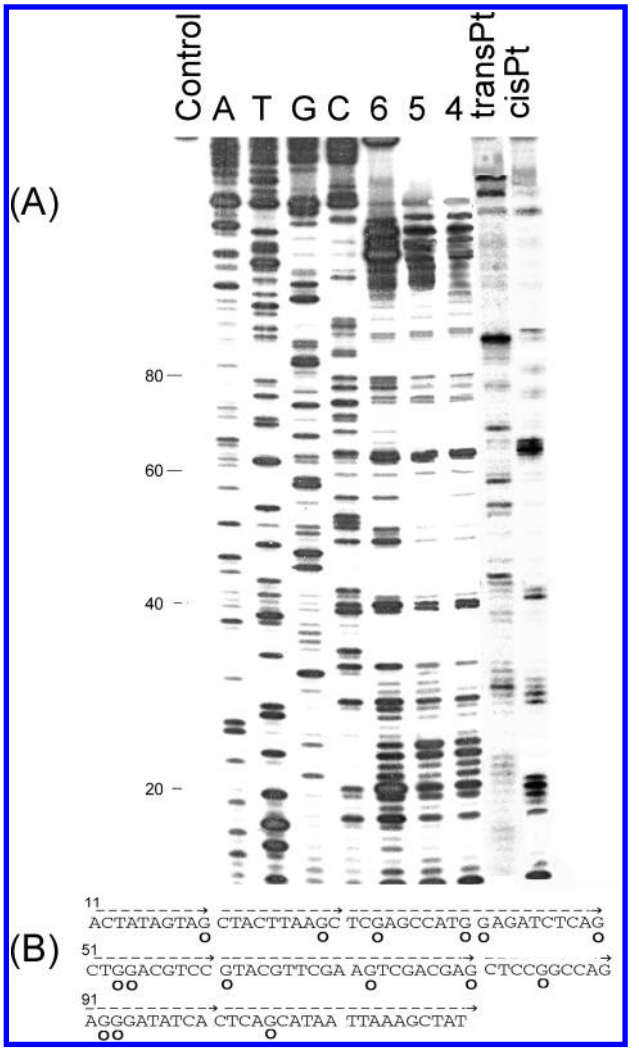

Figure 4. Replication mapping of Ir–DNA adducts. (A) Autoradiogram of 6% polyacrylamide/8 M urea sequencing gel showing inhibition of DNA synthesis by VentR DNA polymerase on the pSP73KB plasmid DNA linearized by *Hpa*I restriction enzyme and subsequently modified by Ir^{III} complexes, cisplatin, or transplatin. Lanes: control, unmodified template; A, T, G, and C, chain-terminated marker DNAs (note that these dideoxy sequencing lanes give the sequence complementary to the template strand); 4–6, DNA modified by complexes **4**–**6** at r_b = 0.01, respectively; cisPt, DNA modified by cisplatin at r_b = 0.01; and transPt, DNA modified by transplatin at r_b = 0.01. The numbers correspond to the nucleotide sequence in panel B. (B) Schematic diagram showing a portion of the sequence used to monitor inhibition of DNA synthesis on the template containing adducts of Ir^{III} complexes. The arrow indicates the direction of the synthesis. ○, major stop signals from panel A, lanes 4–6. The numbering of the nucleotides in this scheme corresponds to the numbering of the nucleotides in the pSP73KB nucleotide sequence map.

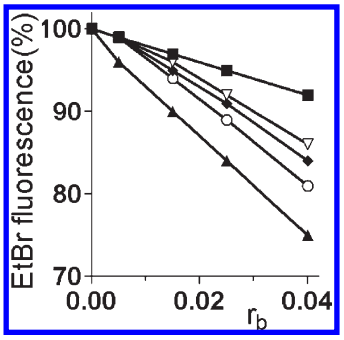

Figure 5. Plots showing the dependence of EtBr fluorescence on r_b for calf thymus DNA modified by Ir^{III} complexes **4**−**6**, cisplatin, and [Pt(dien)Cl]Cl in 10 mM $NaClO_4$ at 310 K for 24 h: complex **4**, ▽; complex **5**, ♦; complex **6**, ○; cisplatin, ▲; and [Pt(dien)Cl]Cl, ■. Data points measured in triplicate varied on average ±3% from their mean.

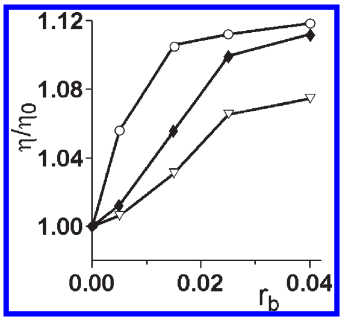

Figure 6. Plots showing the dependence of relative viscosity on r_b for calf thymus DNA modified by Ir^{III} complexes **4**−**6**. The viscosity was measured in 10 mM $NaClO_4$, pH 6, at 310 K. Complex **4**, ▽; complex **5**, ♦; and complex **6**, ○.

DNA for DNA polymerase than cisplatin, and some of them occur at different sequences. These results are consistent with a less regular sequence specificity of complexes **4**−**6** in comparison with cisplatin. Identical patterns of blocks on DNA were observed if the template DNA was incubated with the metal complex for 8, 24, or 72 h (data not shown).

Ethidium Bromide (EtBr) Displacement. The ability of the complexes to displace the DNA intercalator EtBr from CT DNA was probed by monitoring the relative fluorescence of EtBr bound to DNA after treating the DNA with varying concentrations of **4**−**6**. Figure 5 shows a plot of relative fluorescence vs r_b for complexes **4**−**6**, cisplatin, and monofunctional chloridobis(2-aminoethyl)amineplatinum(II) chloride ([Pt(dien)Cl]Cl).

The adducts of monofunctional Ir^{III} complexes competitively replaced intercalated EtBr more effectively than the adducts of monofunctional [Pt(dien)Cl]Cl but slightly less than the adducts of bifunctional cisplatin. Notably, the trend in ability to displace DNA intercalator EtBr from CT DNA was **6** > **5** > **4**, which correlates with their cytotoxicity (Table 4).

Viscometry. The effects of complexes **4**−**6** on the viscosity of rodlike CT DNA (0.15 mg/mL or 0.47 mM in phosphorus content) are shown in Figure 6. On increasing the amounts of **4**−**6** bound to DNA (in the range of r_b values of 0.005−0.04), the relative viscosity of CT DNA increased steadily; the effect follows the order **6** > **5** > **4**, which correlates with their cytotoxicity (Table 4) as well as with their ability to displace DNA intercalator EtBr from DNA (Figure 5).

DISCUSSION

The clinical success of cisplatin and related platinum anticancer drugs[1] has led to the search for active complexes of other transition metals, especially to combat the limited spectrum of activity of platinum, drug resistance, and side effects. Can the design features found in platinum drugs be introduced into other transition metal complexes so as to rationalize the design process? From studies of organometallic half-sandwich arene complexes of the type $[(\eta^6\text{-arene})M(\text{diamine})Cl]^+$ ($M = Ru^{II}$ or Os^{II}), there is evidence that they can.[2c,24] These organometallic complexes contain an M−Cl bond, which can be activated by hydrolysis, and a neighboring NH group can stabilize binding to the nucleobase guanine via NH-C6O H-bonding. Unlike cisplatin, which contains two labile Pt−Cl bonds and can cross-link bases on DNA,[1b] these complexes are monofunctional but nevertheless can cause replication stop-sites when bound to DNA, unlike monofunctional Pt^{II} adducts, such as [Pt(dien)Cl]Cl.[25] Their strong selectivity for G versus A can be reversed by changing the NH group on the chelated ligand (e.g., ethylenediamine) to an H-bond acceptor oxygen such as in acetylacetonate.[26] The interaction of Ru^{II} and Os^{II} arene complexes with DNA and their potency toward cancer cells can be increased by incorporating an extended arene, which can intercalate between base pairs neighboring the metal coordination site.[25,27]

In the present work, we sought to apply these design concepts to Ir^{III} complexes since the biological activity of iridium complexes has received relatively little attention.[6,7] The low-spin d^6 metal ion Ir^{III} is often described in the literature as totally inert, perhaps because water exchange on $[Ir(H_2O)_6]^{3+}$ ions has long been known to take hundreds of years.[5a] On the other hand, it is also known that water exchange in $[(\eta^5\text{-Cp}^*)Ir(H_2O)_3]^{2+}$ is ca. 10^{14} times faster.[28] In general, the dependence of ligand exchange reactions on the nature of the ligands in Ir^{III} complexes has been little studied. We have investigated Ir^{III} complexes containing Cp* ligands since they form highly stable Ir−C bonds, unlike arenes. The catalytic properties of Ir^{III} Cp* complexes have recently been explored.[13,29] We have prepared the Cp* 1,10-phenanthroline complex $[(\eta^5\text{-Cp}^*)Ir(\text{phen})Cl]^+$ (**4**, a complex recently reported to be inactive toward MCF-7 breast and HT-29 colon cancer cells)[30] and compared its aqueous chemistry (hydrolysis and acidity of aqua adduct), nucleobase binding, transcription mapping, cytotoxicity toward A2780 human ovarian cancer cells, hydrophobicity (octanol/water partition), cellular distribution, and DNA intercalation with that of related novel phen complexes containing phenyl- and biphenyl-substituted Cp* ligands (**5** and **6**) and with analogous complexes containing bipyridine (bpy, **7**−**9**) or ethylenediamine (en, **10** and **11**) as the N,N-chelating ligand or picolinate (pico, **12**−**14**) as an N,O-chelating ligand.

Structures of the Complexes. A search of the Cambridge Database revealed that no structure of metal complexes containing the ligand Cp^{xbiph} has been reported. Complex $[(\eta^5\text{-}C_5Me_4C_6H_4C_6H_5)Ir(bpy)Cl]PF_6$ (**9**·PF_6) therefore appears to be the first such structure. The crystal structures of $[(\eta^5\text{-}C_5Me_4C_6H_5)IrCl_2]_2$ (**2**), $[(\eta^5\text{-}C_5Me_4C_6H_5)Ir(phen)Cl]PF_6$ (**5**·PF_6), $[(\eta^5\text{-}C_5Me_4C_6H_5)Ir(bpy)Cl]PF_6$ (**8**·PF_6), $[(\eta^5\text{-}C_5Me_4C_6H_5)Ir(en)Cl]BPh_4$ (**11**·BPh_4), and $[(\eta^5\text{-}C_5Me_4C_6H_5)Ir(pico)Cl]$ (**13**) are the first reported with $(\eta^5\text{-}C_5Me_4C_6H_5)$ (Cp^{xph}) coordinated to iridium.

The bond distances and angles in the dimer $[(\eta^5\text{-}C_5Me_4C_6H_5)IrCl_2]_2$ (**2**) compare well to those found for the corresponding Cp* analogue $[(\eta^5\text{-}C_5Me_5)IrCl_2]_2$ (**1**).[31] The Ir−Cl(bridging)−Ir and Cl(bridging)−Ir−Cl(bridging) angles in **2** are 1.2° more acute and obtuse, respectively, than those of the Cp* analogue. The Ir−Cl

bond lengths in complexes **8**·PF_6 and **9**·PF_6 [2.3859(19) and 2.3840(14) Å, respectively, Table S2 in the Supporting Information] are almost the same; however, the Ir−Cl bond length in complex **7** is slightly longer [2.404(2) Å].[32] The twist angles in complex **9**·PF_6 are similar to those angles in Ru^{II} terphenyl arene complexes.[27c] The Ir−Cl bond length in complex **13** [2.3860(10) Å] is similar to that in complex **12** [(η^5-C_5Me_5)Ir(pico)Cl] [2.3997(15) Å].[33]

The distance between the Ir^{III} and the centroid of Cp ring in [(η^5-$C_5Me_4C_6H_5$)Ir(phen)Cl]PF_6 (**5**·PF_6) (1.783 Å) is similar to that in [(η^5-C_5Me_5)Ir(phen)Cl]CF_3SO_3 (1.780 Å),[34] and the Ir−Cl bond length in **5**·PF_6 (2.3891(5) Å) is similar to that in [(η^5-C_5Me_5)Ir(phen)Cl]CF_3SO_3 (2.395 Å).[34] On changing Cp* to substituted Cp* ligands, no significant change is observed by DFT calculations for Ir−Cl and Ir−cyclopentadienyl ring bond distances. These results suggest that the introduction of phenyl substituent on the Cp* ring does not give rise to significant change in structure.

Hydrolysis and pK_a of Aqua Adducts. There are only a few previous studies of the aquation of organometallic Ir^{III} complexes.[5a,35] In general, all of the complexes studied in this work hydrolyze rapidly. Complexes **4**, **7**, and **10** containing Cp* and **12**−**14** containing picolinate hydrolyzed too rapidly to be observed by conventional UV−vis at 288 K ($t_{1/2}$ < 1 min). Even complex [(η^5-$C_5Me_4C_6H_4C_6H_5$)Ir(phen)Cl]$^+$ (**6**), which hydrolyzed the slowest of these complexes, has a calculated half-life at 310 K of <4 min (Table 1). These results illustrate that Ir^{III} complexes are not always inert and can be quite labile. The hydrolysis of Ir−Cl bonds in iridium complexes is strongly dependent on the coordinated ligands. These Cp^x Ir^{III} complexes undergo even faster hydrolysis than low-spin d^6 arene Ru^{II} and Os^{II} phen complexes,[11a,36] more than 2 orders of magnitude faster than Os^{II} for example. The electron donor methyl groups on the Cp ring may contribute to the fast hydrolysis. These increase the effective charge on Ir and facilitate chloride loss. This behavior is consistent with that of hexamethylbenzene Ru^{II} complexes.[37]

Previous studies on the hydrolysis rates of Os^{II} arene compounds of the type [(η^6-arene)Os(XY)Cl]$^{n+}$ have shown that the aqueous reactivity of these complexes is highly dependent on the nature of the chelating ligand.[38] In particular, the negatively charged electron-donating picolinate ligand increases the rate of hydrolysis as compared to complexes with diamine ligands, as seen here for complexes **12**−**14**.

The presence of bpy as a π-acceptor in complex [(η^6-bip)Ru(bpy)Cl]PF_6, where bip = biphenyl, decreases the rate of hydrolysis by a factor of 2 as compared to the en analogue.[36,39] The π-acceptor ligands bpy and phen can withdraw electron density from a metal center, increasing the positive charge on the metal, making it less favorable for Cl^- to leave, slowing down the hydrolysis. As a result, complexes **5**, **6**, **8**, and **9** containing bpy or phen as the chelating ligand hydrolyzed much more slowly than the en complex **10** and pico analogues, complexes **13** and **14**. However, despite the electron-withdrawing ability of bpy and phen, the hydrolysis rates of complexes **4** and **7** are still relatively fast and appear to be controlled by the powerful electron donor Cp*.

Our previous work has shown that the interaction of [(η^6-bip)Ru(en)Cl]$^+$ with amino acids,[40] proteins,[40] peptides,[41] and DNA bases[11b] involves aquation (substitution of Cl by H_2O) as the first step. The anticancer drug cisplatin also undergoes aquation prior to platination of the target site, DNA.[18b,42] The equilibrium constants at 278 K for hydrolysis of complexes **4**−**6**, **7**−**9**, and **12**−**14**, decrease in the order **6** > **5** > **4**, **9** > **8** > **7**, and **14** > **12**, **13** (Table 1), which parallels their cytotoxicity (Table 4), perhaps indicating that activation by aquation is important for the mechanism of their cytotoxic action.

At chloride concentrations typical of blood plasma (104 mM) and cell cytoplasm (23 mM), the inactive complex [(η^5-C_5Me_5)-Ir(bpy)Cl]$^+$ (**7**) (IC_{50} > 100 μM, Table 4) was found to be almost all present in solution as the intact chlorido species, which is relatively unreactive as compared to the aqua complex **7A**. At a chloride concentration of 4 mM, close to that of the cell nucleus, only about 5% of **7** was present as the reactive aqua species.

When the pK_a values of the aqua complexes (Table 2) are compared, it is evident that the presence of phenyl or biphenyl substitutent lowers the pK_a value by ca. 0.4 units consistent with withdrawal of electron density from the Ir center. Replacement of the π-acceptor ligand bpy in aqua complex **7A** by the chelating diamine donor en to give **10A** leads to a significant increase in pK_a by ca. 0.7 units, consistent with an increased electron density on the metal center. Similarly, the replacement of the neutral chelated bpy ligand by the anionic pico ligand raises the pK_a by 1.1 units. There appears to be no correlation between the pK_a values of the aqua adducts and the cytotoxicity of these complexes. The pK_a values of the pico, en, and phen aqua complexes **4A**, **6A**, **10A**, **12A**−**14A** suggest that they will be present largely as the reactive aqua adducts as opposed to the less reactive hydroxo adducts at physiological pH (7.4), whereas the pK_a values of the bpy complexes **7A**−**9A** are significantly lower, especially **8A**, and therefore most of the hydrolyzed bpy complexes would be present as the hydroxido form (at pH 7.4). Despite this, complexes **8** and **9** exhibit good activity. Their reactivity would be aided by the small lowering of pH, which is thought to occur in tumors.[43]

For Ru^{II} complexes that contain biphenyl as the arene and bpy as chelating ligand, loss of the arene is observed in aqueous solution.[36] In contrast, no loss of any Cp^x ligands was observed for any of the Ir^{III} complexes studied in this work.

Interactions with Nucleobases. DNA is often a target for cytotoxic transition metal anticancer complexes.[21] There is little reported work on interactions of iridium complexes with nucleobases.[44] In the present study, the reactions of complexes **4**−**14** and aqua complex **5A** with 9-EtG and 9-EtA were investigated. Complexes **4**−**11** and **5A** containing a neutral N, N-chelating ligand all bind selectively to 9-EtG as compared to 9-EtA, with which no reaction was observed after 24 h. This result is consistent with the replication mapping experiments (Figure 4), which show that G residues are the preferential binding sites on polymeric DNA modified with complexes **4**−**6**. The less regular sequence specificity of complexes **4**−**6** in comparison with cisplatin might arise from the faster DNA binding of **4**−**6**. The selectivity in nucleobase binding can be rationalized in terms of H-bonding, nonbonding repulsive interactions between the chelating ligand and the nucleobase substituents, and the electronic properties of the various nucleobase coordination sites.[38a] Our previous studies of Ru−N7 guanine adducts have revealed a strong H-bonding interaction between one en NH and G C6O.[11b] This may explain the strong affinity of 9-EtG for the Ir^{III} en complexes **10** and **11**. A phenanthroline ligand cannot provide a donor NH group, but instead, the interaction with G C6O may be stabilized by a C−H H-bond similar to that observed in a bipyridine complex of Ru^{II}.[36] This possibility was indicated by the DFT optimized structure of the 9-EtG adduct of **6** (Figure S18 and Table S5 in the Supporting Information).

Complexes **4**−**11** containing an N,N-chelating ligand did not react with 9-EtA, most likely due to the steric hindrance of the NH_2 group on the 6-position of the adenine ring. As compared to complexes containing an N,N-chelating ligand, compounds **12**−**14** that contain the N,O-chelating ligand pico bind significantly (70−100%) to both nucleobases; see Table 3. These picolinate Ir^{III} adducts of complexes **12**−**14** with 9-EtA (**12Ad**, **13Ad**, and **14Ad**, respectively) can be stabilized by hydrogen bonding between the NH_2 group of adenine and a carboxylate oxygen of the picolinate ligand.[45] As expected, the aqua complex **5A** reacted to a greater extent with 9-EtG as compared to the chlorido complex **5**, see Table 3, consistent with the increased reactivity of aqua adducts as compared to their chlorido forms,[18a] but the selectivity for G versus A was the same.

Hydrophobicity (log *P*) and Cell Accumulation. log *P* values for octanol/water partition provide a measure of hydrophobicity that is often a factor relevant for cell uptake and anticancer activity. For several classes of metallo-anticancer complexes, a correlation between increased hydrophobicity and increased cytotoxic activity has been reported.[22,23]

In this study, as expected, the log *P* values (Table 5) and hydrophobicity increase with increasing size of the substituted Cp* ligand. Additionally, the hydrophobicity, cancer cell activity, and cell accumulation correlate significantly, following the order **6** > **5** > **4**. Complex $[(\eta^5\text{-}C_5Me_5)Ir(phen)Cl]^+$ (**4**) is the least hydrophobic, the least cytotoxic, and the least taken up by the cells, whereas complex $[(\eta^5\text{-}C_5Me_4C_6H_4C_6H_5)Ir(phen)Cl]^+$ (**6**) displays the highest hydrophobicity, is the most cytotoxic, and the most taken up by the cells. These data suggest that in the ovarian A2780 cancer cell line, the log *P* value is a useful parameter for predicting the cytotoxicity of this class of iridium complexes. These data also show that using more extended coordinated Cp^x ligands such as Cp^{xbiph} gives rise to an increased hydrophobicity, leading to higher cellular uptake and higher cytotoxicity. For Os^{II} arene complexes, this range of log *P* values (−0.51 and 0.86) is also accompanied by promising anticancer activity.[46] Such complexes are hydrophobic enough to partition efficiently into cells and yet hydrophilic enough to exhibit reasonable aqueous solubility.

Distribution of Iridium in Cells. The accumulation of the three phen complexes **4**−**6** into the different cell fractions was studied. A significant proportion of the total iridium (54−74%) was in the cell membrane fraction; see Figure 3. This may be related not only to Ir being transported into the cytoplasm but also to Ir being exported by cells. For all complexes, the next highest concentration of iridium was found in the cytosol showing that passage through the outer membrane readily occurs.

Although the lowest proportion of iridium was found in the nucleus, especially for complexes **4** and **6**, it is notable that there is a correlation between nucleus accumulation and cytotoxicity of the complexes, both of which follow the order **6** > **5** > **4**, suggesting that penetrating the nucleus and binding to nuclear DNA may provide an important contribution to the mechanism of cytotoxicity. A similar relationship between nucleus accumulation and cytotoxicity was observed for Os^{II} arene complexes.[46]

DNA Binding in A2780 Carcinoma Cells. The amount of iridium found on the DNA of A2780 cells (Table 6) incubated with the complexes for 24 h follows the order **6** > **5** > **4**, which correlates with their cytotoxicity, hydrophobicity (log *P*), and cellular accumulation (Table 6) and is similar to the total accumulation by cell nuclei. The extent of iridium binding of **4**−**6** to DNA, 5.5−7.7% of the total iridium taken up by the cells, is higher than that reported for cisplatin (∼1%)[47] and Os^{II} arene complexes.[46] DNA may therefore be a potential target for these cytotoxic iridium complexes, although we cannot rule out the possibility that nuclear DNA may not be the only target.[48]

EtBr Displacement and Viscometry. The fluorescent probe EtBr can be used to distinguish between intercalating and nonintercalating ligands.[25,49] Viscosity measurements are also useful for probing the nature of DNA interactions since viscosity is sensitive to alterations in DNA length. For instance, complexes or ligands that intercalate cause an increase in overall DNA contour length due to the increase in separation of base pairs at the intercalation sites, which leads to an increase in viscosity of DNA solutions. On the other hand, drug molecules that bind in DNA grooves cause less pronounced changes in the viscosity of DNA solutions.[50]

Modification of CT DNA by complexes **4**−**6** resulted in a decrease of EtBr fluorescence intensity (Figure 5) and an increase in the relative viscosity of CT DNA (Figure 6) in the same order **6** > **5** > **4**, which correlates with their cytotoxicity (IC_{50} values). These results indicate that addition of phenyl substituents to the Cp* ring in these iridium complexes enhances the intercalative ability into DNA. Dual-mode intercalation/G N7 coordination DNA binding may therefore play an important role in the cytotoxicity of these Ir^{III} complexes. This observation parallels that of Ru^{II} and Os^{II} arene complexes for which extended arenes can also intercalate and increase the potency of the complexes.[12a,24c] For example, the Ru^{II} anticancer complex $[(\eta^6\text{-}p\text{-terp})Ru(en)Cl]^+$ (where *p*-terp = *para*-terphenyl, a similar arene ligand to Cp^{xbiph}) also exhibits combined intercalative and monofunctional (coordination) binding to DNA.[27c]

The DFT-computed EPSs of the phen complexes **4**−**6** show more positive values than those of pico complexes **12**−**14** (same trend for the aqua derivatives **6A** and **14A**). This may favor interaction with negatively charged DNA in the case of phen complexes. The higher electron density on the second phenyl ring of the Cp^{xbiph} ligands (Figure 2), together with the lower steric hindrance of the terminal phenyl ring, can explain the better intercalation properties of **6**. Complex **6** is likely to be present in the nucleus largely as the aqua complex **6A**, which has an even higher positive charge distributed over its surface (Figure 2).

Cytotoxicity. Complexes $[(\eta^5\text{-}C_5Me_5)Ir(phen)Cl]Cl$ (**4**·Cl), $[(\eta^5\text{-}C_5Me_5)Ir(bpy)Cl]Cl$ (**7**·Cl), $[(\eta^5\text{-}C_5Me_5)Ir(en)Cl]PF_6$ (**10**·PF_6), and $[(\eta^5\text{-}C_5Me_5)Ir(pico)]$ (**12**) containing Cp* were nontoxic (IC_{50} > 100 μM) toward the human ovarian A2780 cancer cell line (Table 4). The cytotoxicity of complexes $[(\eta^5\text{-}C_5Me_4C_6H_5)Ir(phen)Cl]PF_6$ (**5**·PF_6) and $[(\eta^5\text{-}C_5Me_4C_6H_4C_6H_5)Ir(phen)Cl]PF_6$ (**6**·PF_6) containing phenyl and biphenyl substituents, respectively, on the tetramethylcyclopentadienyl ring increases dramatically as compared to the parent Cp* complex **4**. Complex **6** containing Cp^{xbiph} is ca. twice as potent toward A2780 human ovarian cancer cells as the anticancer drug cisplatin (Table 4). The introduction of phenyl and biphenyl substituents also resulted in significant increases in activity for complexes **7**−**9**, **10**−**11**, and **12**−**14**, suggesting that these phenyl groups play a crucial role in the mechanism of action. This is consistent with our previous observations that the cytotoxicity of η^6-arene Ru^{II} compounds increases with the size of the arene ring system in the order benzene < *p*-cymene < biphenyl < dihydroanthracene < tetrahydroanthracene.[3c] The increase in potency on addition of phenyl substituents to the Cp ring, by about an order of magnitude for each of the additions (from **4** to **5** to **6**), is more dramatic than in the case of ruthenium arene

ethylenediamine complexes.[27c,51] For these iridium complexes, the phenyl substitutents not only enhance lipophilicity and cell accumulation but also introduce an additional mode of DNA interaction (intercalation).

Both complexes $[(\eta^5\text{-}C_5Me_4C_6H_5)Ir(bpy)Cl]^+$ (**8**) and $[(\eta^5\text{-}C_5Me_4C_6H_5)Ir(pico)Cl]$ (**13**) contain Cp^{xph}, however, **8** exhibits activity toward A2780 cancer cells whereas **13** is inactive, which suggests that the chelating ligand also plays a role. Replacement of neutral bpy by anionic pico as the chelating ligand increases the rate and extent of hydrolysis, the pK_a of the aqua complex (from 6.31 to 7.75 for ring = Cp^{xph}, Table 2), and changes the nucleobase specificity. For complexes **7**−**9** containing neutral bpy, there is exclusive binding to 9-EtG. In contrast, complexes **12**−**14**, containing anionic pico, bind strongly to both 9-EtG and 9-EtA. These results are in agreement with previous work on Ru^{II} and Os^{II} complexes in which neutral en is replaced by negatively charged acetylacetonate (acac).[26,38a] The rapid hydrolysis, low acidity of aqua adducts, and strong binding to biomolecules may account for the low cytotoxicity of the picolinate complexes. The highly reactive aqua species may interact with other cellular biomolecules before they reach target sites, thus effectively being deactivated. For example, the amino acids (methionine or cysteine) or tripeptides can form S-bound adducts with Ir^{III} Cp* complexes.[44a]

Interestingly, some ruthenium[27a] and osmium[11a] arene complexes containing phen or bpy derivatives show poor or no activity against A2780 cells. The inactivity of phen complex **4** and bpy complex **7** may be correlated with their low extent of hydrolysis and poor cellular accumulation. Although complex **7** may reach the cell nucleus, its hydrolysis is largely suppressed (only 5% hydrolyzed in the presence of 4 mM NaCl), and the complex therefore remains predominately as the less-reactive intact chlorido species. These factors may explain the inactivity of **4** and **7** and also the inactivity of **10**.

■ CONCLUSIONS

The goal of the present study was to explore the rational design of monofunctional organometallic half-sandwich Ir^{III} anticancer complexes based on knowledge of the features that contribute to the activity of half-sandwich Ru^{II} and Os^{II} arene complexes.[2,24a,52] The biological and medicinal chemistry of iridium complexes has been little explored previously,[6,7] perhaps because it is often assumed that low-spin $5d^6$ Ir^{III} complexes are highly kinetically inert.[5,9,10] Our data show that this is not always the case. Cyclopentadienyl ligands, while stabilizing Ir^{III}, can confer kinetic lability on trans monodentate ligands such as chloride. Moreover, phenyl substituents on the Cp* ring as in Cp^{xph} and Cp^{xbiph} can have a major effect on the chemical and biological behavior of $[(\eta^5\text{-}Cp^x)Ir(XY)Cl]^{0/+}$ complexes.

This appears to be the first time that Cp^{xph} and Cp^{xbiph} ligands have been used in iridium complexes. The crystal structure of complex $[(\eta^5\text{-}C_5Me_4C_6H_4C_6H_5)Ir(bpy)Cl]PF_6$ (**9**·PF_6) appears to be the first reported structure containing the ligand Cp^{xbiph}. The crystal structures of $[(\eta^5\text{-}C_5Me_4C_6H_5)IrCl_2]_2$ (**2**), $[(\eta^5\text{-}C_5Me_4C_6H_5)Ir(phen)Cl]PF_6$ (**5**·PF_6), $[(\eta^5\text{-}C_5Me_4C_6H_5)Ir(bpy)Cl]PF_6$ (**8**·PF_6), $[(\eta^5\text{-}C_5Me_4C_6H_5)Ir(en)Cl]BPh_4$ (**11**·BPh_4), and $[(\eta^5\text{-}C_5Me_4C_6H_5)Ir(pico)Cl]$ (**13**) are the first to be reported with η^5-$C_5Me_4C_6H_5$ coordinated to iridium.

Figure 7 provides an overview of the relationships between cancer cell cytotoxicity, intercalative ability, cellular accumulation, hydrophobicity, and rates and extents of hydrolysis for the phen

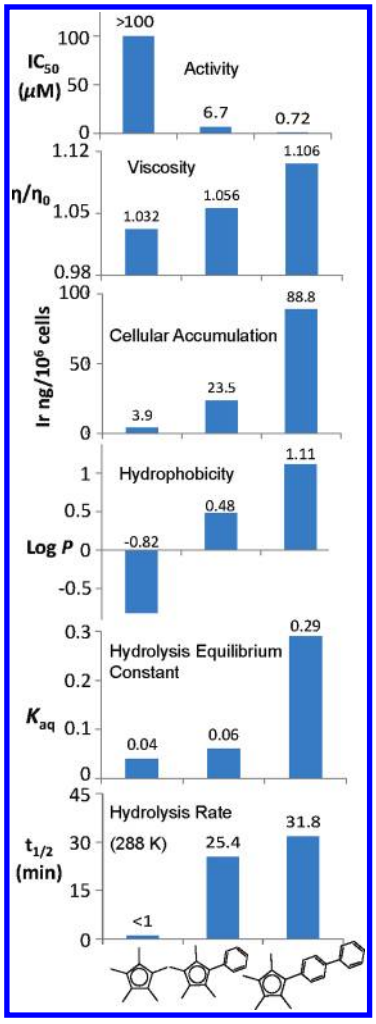

Figure 7. Bar charts illustrating the relationship between cytotoxicity toward human cancer cells, intercalative ability, cellular accumulation, hydrophobicity, and rates (288 K) and equilibrium constants (278 K) of hydrolysis for iridium complexes $[(\eta^5\text{-}Cp^x)Ir(phen)Cl]^+$ containing Cp^x = Cp* (**4**), Cp^{xph} (**5**), and Cp^{xbiph} (**6**).

complexes **4**−**6**. Figure 8 shows how the chelating and Cp^x ligands affect the anticancer activity, nucleobase binding, and aqueous chemistry of the bpy complexes **7**−**9** and pico complexes **12**−**14**. These $[(\eta^5\text{-}Cp^x)Ir(XY)Cl]^{0/+}$ complexes hydrolyze rapidly (the slowest half-life <4 min at 310 K), and the nature of the cyclopentadienyl and chelating ligands significantly influence their aqueous chemistry. In general, the introduction of phenyl and biphenyl Cp* ring substituents slows down the hydrolysis rate, increases the extent of hydrolysis, and increases the acidity of the respective aqua species. The chelating ligand appears to determine the selectivity of nucleobase binding. The complexes containing N,N-chelating ligands discriminate strongly between the purine nucleobases guanine and adenine, showing little binding to the latter for either for Cp*, Cp^{xph}, or Cp^{xbiph} complexes. In contrast, complexes **12**−**14** containing the N,O-chelating ligand picolinate bind to both 9-EtG and 9-EtA.

The introduction of a phenyl substituent into the Cp* ring switches on cancer cell cytotoxicity. For example, the tetramethyl(phenyl)-cyclopentadienyl complex **5** is more than 1 order of magnitude more potent than the Cp* complex **4**, and the biphenyl complex **6** is more than 2 orders of magnitude more potent than complex **4** and twice as potent as cisplatin in the same cell line. This increase in activity

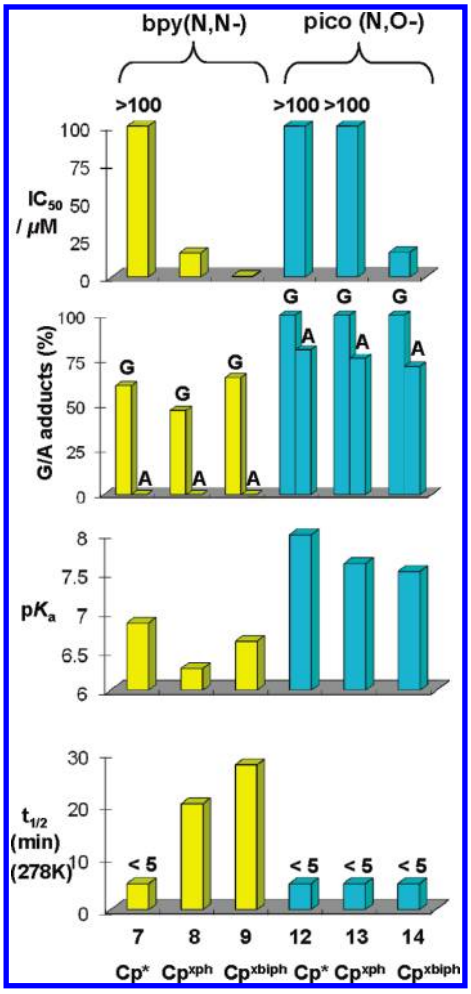

Figure 8. Bar charts illustrating the influence of N,N- and N,O-chelating ligands on the cytotoxicity, nucleobase binding, hydrolysis, and pK_a of the aqua adducts of the bpy complexes **7**−**9** and pico complexes **12**−**14**.

parallels the increase in hydrophobicity, increase in cell accumulation, and DNA binding. Complexes **5** and **6** can exhibit dual mode binding to DNA: iridium binding to G N7 is accompanied by intercalation of the phenyl substituents on the Cp* ring. Significant increases in activity for complexes **7**−**9**, **10**−**11**, and **12**−**14** are also observed. On the other hand, the chelating ligand can also play an important role in the anticancer activity. For example, the pico complex **13** shows no activity toward the A2780 cell line, while the bpy analogue complex **8** shows good activity, and the bpy complex **9** is more than 1 order of magnitude more potent than the pico analogue, complex **14**.

The work reported here demonstrates that rational chemical design can be applied to Ir^{III} complexes to achieve potent cancer cell cytotoxicity. It is notable that Cp ring substituents can also play a major role in controlling the chemical and biological properties of ferrocenyl and titanocenyl anticancer complexes.[53] In general, organometallic complexes offer much promise for the design of novel therapeutic agents.[2,24a,52a]

EXPERIMENTAL SECTION

Details of the materials used and the synthesis and characterization of complexes are in the Supporting Information. The general synthetic route to the iridium complexes involved reaction of 1,10-phenanthroline, 2,2′-bipyridine, ethylenediamine, or 2-picolinate, with the appropriate dimer $[(\eta^5\text{-}Cp^x)IrCl_2]_2$ in methanol. CHN elemental analyses were carried out for all complexes and synthesized ligands, by which their purities were confirmed to be in excess of 97.0%.

Methods and Instrumentation. *X-ray Crystallography.* All diffraction data were obtained on an Oxford Diffraction Gemini four-circle system with a Ruby CCD area detector using Mo Kα radiation. Absorption corrections were applied using ABSPACK.[54] The crystals were mounted in oil and held at 100(2) K with the Oxford Cryosystem Cobra. The structures were solved by direct methods using SHELXS (TREF)[55] with additional light atoms found by Fourier methods. Complexes were refined against F^2 using SHELXL,[56] and hydrogen atoms were added at calculated positions and refined riding on their parent atoms.

X-ray crystallographic data for complexes **2**, **5**·PF_6, **8**·PF_6, **9**·PF_6, **11**·BPh_4, and **13** are available as Supporting Information and have been deposited in the Cambridge Crystallographic Data Centre under the accession numbers CCDC 802289, 802288, 802287, 802291, 802290, and 802286, respectively. X-ray crystallographic data in CIF format are available from the Cambridge Crystallographic Data Centre (http://www.ccdc.cam.ac.uk/).

NMR Spectroscopy. ^{1}H NMR spectra were acquired in 5 mm NMR tubes at 298 K (unless stated otherwise) on either Bruker DPX 400 (^{1}H = 400.03 MHz) or AVA 600 (^{1}H = 600.13 MHz) spectrometers. ^{1}H NMR chemical shifts were internally referenced to $(CHD_2)(CD_3)SO$ (2.50 ppm) for DMSO-d_6, $CHCl_3$ (7.26 ppm) for chloroform-d_1, or to 1,4-dioxane (3.75 ppm) for aqueous solutions. All data processing was carried out using XWIN-NMR version 3.6 (Bruker UK Ltd.).

Mass Spectrometry. Electrospray ionization mass spectra (ESI-MS) were obtained by preparing the samples in 50% CH_3CN and 50% H_2O (v/v) and infusing into the mass spectrometer (Bruker Esquire 2000). The mass spectra were recorded with a scan range of m/z 50−1000 for positive ions.

Elemental Analysis. CHN elemental analyses were carried out on a CE-440 elemental analyzer by Exeter Analytical (UK) Ltd.

pH Measurement. pH* values (pH meter reading without correction for effects of deuterium on glass electrode) of NMR samples in D_2O were measured at ca. 298 K directly in the NMR tube, before and after recording NMR spectra, using a Corning 240 pH meter equipped with a microcombination electrode calibrated with Aldrich buffer solutions of pH 4, 7, and 10.

UV−vis Spectroscopy. A Cary 300 UV−vis recording spectrophotometer was used with 1 cm path-length quartz cuvettes (0.5 mL) and a PTP1 Peltier temperature controller. Spectra were processed using UVWinlab software. Experiments were carried out at 288 K unless otherwise stated.

Kinetics of Hydrolysis. Solutions of complexes **4**−**10** and **12**−**14** with final concentrations of 0.2−0.7 mM in 5% MeOD-d_4/95% D_2O (v/v) were prepared by dissolution of the complexes in MeOD-d_4 followed by rapid dilution with D_2O. ^{1}H NMR spectra were recorded after various time intervals. The rates of hydrolysis were determined by fitting plots of concentrations (determined from ^{1}H NMR peak integrals) versus time to a first-order rate equation using ORIGIN version 8.1. The hydrolysis of complexes **4**, **7**, **10**, **12**−**14** was monitored by ^{1}H NMR at 278 K (to slow down the rate and avoid freezing the samples) and for complexes **5**, **6**, **8**, and **9** at 278, 283, 288, and 293 K. The Arrhenius equation $\ln(k) = \ln(A) - E_a/RT$ was used to calculate the hydrolysis rate constants and half-lives of **5**, **6**, **8**, and **9** at 310 K.

Determination of pK_a Values. To generate the aqua complexes, chlorido complexes were dissolved in D_2O, and 0.98 mol equiv of $AgNO_3$ were added. The solution was stirred for 24 h at 298 K, and AgCl was removed by filtration. For determinations of pK_a* values (pK_a values for solutions in D_2O), the pH* values of solutions of the aqua complexes in this study in D_2O were varied from ca. pH* 2 to 11 by the addition of dilute NaOD and $DClO_4$, and ^{1}H NMR spectra were recorded. The chemical shifts of the chelating ligand protons and/or methyl protons of

dx.doi.org/10.1021/jm2000932 |J. Med. Chem. 2011, 54, 3011–3026

Cp^x were plotted against pH*. The pH* titration curves were fitted to the Henderson−Hasselbalch equation, with the assumption that the observed chemical shifts are weighted averages according to the populations of the protonated and deprotonated species. These pK_a* values can be converted to pK_a values by use of the equation $pK_a = 0.929pK_a^* + 0.42$ as suggested by Krezel and Bal[20] for comparison with related values in the literature.

Computational Details. The Gaussian 03 package[57] was employed for all calculations. Geometry optimization calculations for complexes **4**−**14**, aqua complexes **6A** and **14A**, and 9-EtG adduct **7G** were performed in the gas phase with the gradient-corrected correlation functional PBE0.[58] The LanL2DZ basis set and effective core potential[59] were used for the Ir atom, and the 6-31G** basis set was used for all other atoms.[60] The nature of all stationary points was confirmed by performing a normal-mode analysis. EPSs for complexes **4**−**6**, **12**−**14**, **6A**, and **14A** were calculated and mapped on electron density (isovalue 0.004) of the molecules. The electrostatic potential is represented with a color scale ranging from red (−0.100 au) to blue (0.150 au).

Interactions with Nucleobases. The reaction of complexes **4**−**14** and **5A** (ca. 1 mM) with nucleobases typically involved addition of a solution containing 1 mol equiv of nucleobase in D_2O to an equilibrium solution of complexes **4**−**14** in 5% MeOD-d_4/95% D_2O (v/v) or to a solution of the aqua complex **5A** (prepared by the addition of 1 mol equiv of $AgNO_3$ to a solution of **5** and removal of AgCl by filtration). ^{1}H NMR spectra of these solutions were recorded at 310 K after various time intervals.

Inductively Coupled Plasma−Mass Spectrometry (ICP-MS) Instrumentation and Calibration. All ICP-MS analyses were carried out on an Agilent Technologies 7500 series ICP-MS instrument. The water used for ICP-MS analysis was doubly deionized (DDW) using a Millipore Milli-Q water purification system and a USF Elga UHQ water deionizer. The iridium Specpure plasma standard (Alfa Aesar, 1000 ppm in 10% HCl) was diluted with 3% HNO_3 DDW to freshly prepare calibrants at concentrations 1000, 800, 400, 200, 100, 50, 10, 1, and 0.1 ppb. The ICP-MS instrument was set to detect ^{193}Ir with typical detection limits of ca. 8 ppt using no-gas mode.

Cell Culture and Cytotoxicity. The A2780 ovarian cell line was obtained from the ECACC (European Collection of Animal Cell Culture, Salisbury, United Kingdom). The cells were maintained in RPMI 1640 media, which was supplemented with 10% fetal calf serum, 1% L-glutamine, and 1% penicillin/streptomycin. All cells were grown at 310 K in a humidified atmosphere containing 5% CO_2.

Stock solutions of the Ir^{III} complexes were first prepared in DMSO to assist dissolution and then diluted into 0.9% saline and medium (1:1). After plating 5000 A2780 cells per well on day 1, Ir^{III} complexes were added to the cancer cells on day 3 at concentrations ranging from 0.05 to 100 μM, depending on the preliminary activity data obtained in screening assays. Cells were exposed to the complexes for 24 h, washed with PBS, supplied with fresh medium, and allowed to grow for three doubling times (72 h), and then the protein content (proportional to cell survival) measured using the sulforhodamine B (SRB) assay.[61] The standard errors are based on two independent experiments of three replicates each.

log P Determination. Octanol-saturated water (OSW) and water-saturated octanol (WSO) were prepared using analytical grade octanol and 0.2 M aqueous NaCl solution (to suppress hydrolysis of the chlorido complexes). Aliquots of stock solutions of iridium complexes in OSW were added to equal volumes of WSO and shaken in an IKA Vibrax VXC basic shaker for 4 h at 500 g/min to allow partition at ambient temperature (~298 K). The aqueous layer was carefully separated from the octanol layer for iridium analysis. ^{193}Ir was quantified from aliquots taken from the octanol-saturated aqueous samples before and after partition. Partition coefficients of Ir^{III} complexes were calculated using the equation $\log P = \log([Ir]_{WSO}/[Ir]_{OSW})$, where $[Ir]_{WSO}$ was obtained by subtraction of the Ir content of the aqueous layer after partition from the Ir content of the aqueous layer before partition.

Cell Accumulation, Cellular Distribution, and DNA Binding in A2780 Human Carcinoma Cells. A2780 cells were plated at a density of 5×10^6 cells/100 mm Petri dish in 9 mL of culture medium on day 1 (three dishes were prepared per compound tested, and three untreated control dishes, in two independent experiments). On day 2, cells were exposed to the Ir^{III} complexes **4**−**6**. Stock solutions of the iridium compounds were prepared fresh in DMSO and diluted in 0.9% saline and medium (1:1; 0.5% v/v DMSO final concentration) to a final concentration of Ir on the plates of 5 μM. After 24 h of drug exposure at 310 K on a 5% CO_2 incubator, the drug-containing medium was removed, and the cells were washed, trypsinized, and counted using a hemocytometer. One-third of the cells were centrifuged, quickly washed with PBS, and stored at 253 K for determination of total cell accumulation (the net effect of uptake and efflux) of iridium. Another third of the samples was used for cytosol, nucleus, membrane/particulate, and cytoskeleton fractionation, using a FractionPREP cell fractionation kit from BioVision (Mountain View, CA). The last third of the samples was used for quantification of Ir bound to DNA using the Nucleon genomic DNA extraction kit (GE healthcare, Amersham, United Kingdom; BACC-1 protocol). All of the cell pellets and solid cell fractions were digested in freshly distilled 72% HNO_3 in Wheaton V-Vials with a PTFE-faced rubber-lined cap (Sigma-Aldrich) for 16 h at 373 K. After they were cooled, the samples were diluted with DDW to a maximum final concentration of 7.2% HNO_3 (suitable for ICP-MS analysis) prior to quantification of iridium.

Sequence Preference of DNA Adducts. The primer extension footprinting assay was used to evaluate the sequence selectivity of DNA modification by complexes **4**−**6**. A fragment of pSP73KB DNA linearized by *Hpa*I (2464 bp) was incubated with Ir^{III} complexes in 10 mM $NaClO_4$ for 24 h at 310 K to obtain $r_b = 0.01$ (bound Ir/base). The excess of drug was removed by ethanol precipitation. Circum VentTM Thermal Cycle Sequencing Kit with Vent(exo$^-$) DNA polymerase was used along with the protocol for thermal cycle DNA sequencing with 5′-end-labeled 20-mer SP6 primer recommended by the manufacturer with small modifications.[62] The synthesis products were separated by electrophoresis on a denaturing polyacrylamide (PAA) gel [6% polyacrylamide (PAA)/8 M urea]; sequence ladders were obtained in parallel using untreated control DNA fragments.

Fluorescence Measurements. These measurements were performed on a Shimadzu RF 40 spectrofluorophotometer using a 1 cm quartz cell. Fluorescence measurements of CT DNA modified by Ir^{III} complexes, cisplatin, or [Pt(dien)Cl]Cl (dien = diethylenetriamine), in the presence of EtBr, were performed at an excitation wavelength of 546 nm, and the emitted fluorescence was analyzed at 590 nm. The fluorescence intensity was measured at 298 K in 0.4 M NaCl to avoid secondary binding of EtBr to DNA.[63] The concentrations were 0.01 mg/mL for DNA and 0.04 mg/mL for EtBr, which corresponded to the saturation of all intercalation sites for EtBr on DNA.[63a]

Viscometry. The relative viscosity of the solutions of CT DNA nonmodified or modified by complexes **4**−**6** at the concentration of 150 μg/mL was measured by microviscometry (AMVn Automated Micro Viscometer, Anton Paar GmbH, Austria) using a 1.6 mm capillary tube at 310 K. The densities of the solutions were measured using a Density Meter DMA 4500 instrument (Anton Paar GmbH, Austria).

■ ASSOCIATED CONTENT

Supporting Information. Details of the materials used, synthesis and characterization of ligands and complexes, crystallographic data (Tables S1 and S2 and Figures S1−S4), calculations (Tables S3, S4, S6, and S18), aqueous chemistry (Figures S5−S12), nucleobase studies (Figures S13−S17), and

distribution in cell fractions (Table S5). This material is available free of charge via the Internet at http://pubs.acs.org.

AUTHOR INFORMATION

Corresponding Author

*Tel: (+44)024 7652 3818. Fax: (+44)024 7652 3819. E-mail: p.j.sadler@warwick.ac.uk.

Present Addresses

[§]Utrecht University.

ACKNOWLEDGMENT

Z.L. was supported by a University of Warwick Research Scholarship. L.S. was supported by ERC BIOINCMED and MC-IEF (L.S. 220281 PHOTORUACD), P.C.A.B. was supported by The Netherlands Organisation for Scientific Research through a Rubicon Scholarship, and A.K. and V.B. were supported by the Czech National Foundation (Grant nos. P303/11/P047 and P301/10/0598). We thank the ERC (Grant no. 247450 for P.J.S.), EPSRC, ORSAS, and ERDF and AWM for Science City funding and members of COST Action D39 for stimulating discussions.

ABBREVIATIONS USED

Cp*, pentamethylcyclopentadienyl; Cp^{xph}, tetramethyl(phenyl)-cyclopentadienyl; Cp^{xbiph}, tetramethyl(biphenyl)cyclopentadienyl; 9-EtG, 9-ethylguanine; 9-EtA, 9-ethyladenine; IC_{50}, half-maximum inhibitory concentration

REFERENCES

(1) (a) Kelland, L. The Resurgence of Platinum-Based Cancer Chemotherapy. *Nat. Rev. Cancer* **2007**, *7*, 573–584. (b) Wang, D.; Lippard, S. J. Cellular Processing of Platinum Anticancer Drugs. *Nat. Rev. Drug Discovery* **2005**, *4*, 307–320.

(2) (a) Halpern, J. Organometallic Chemistry at the Threshold of a New Millennium. Retrospect and Prospect. *Pure Appl. Chem.* **2001**, *73*, 209–220. (b) Fish, R. H.; Jaouen, G. Bioorganometallic Chemistry: Structural Diversity of Organometallic Complexes with Bioligands and Molecular Recognition Studies of Several Supramolecular Hosts with Biomolecules, Alkali-Metal Ions, and Organometallic Pharmaceuticals. *Organometallics* **2003**, *22*, 2166–2177. (c) *Medicinal Organometallic Chemistry (Topics in Organometallic Chemistry)*, 1st ed.; Jaouen, G., Metzler-Nolte, N., Eds.; Springer-Verlag: Heidelberg, Germany, 2010; Vol. 32. (d) Hartinger, C. G.; Dyson, P. J. Bioorganometallic Chemistry—From Teaching Paradigms to Medicinal Applications. *Chem. Soc. Rev.* **2009**, *38*, 391–401. (e) Yan, Y. K.; Melchart, M.; Habtemariam, A.; Sadler, P. J. Organometallic Chemistry, Biology and Medicine: Ruthenium Arene Anticancer Complexes. *Chem. Commun.* **2005**, 4764–4776. (f) Suss-Fink, G. Arene Ruthenium Complexes as Anticancer Agents. *Dalton Trans.* **2010**, *39*, 1673–1688.

(3) (a) Mendoza-Ferri, M. G.; Hartinger, C. G.; Mendoza, M. A.; Groessl, M.; Egger, A. E.; Eichinger, R. E.; Mangrum, J. B.; Farrell, N. P.; Maruszak, M.; Bednarski, P. J.; Klein, F.; Jakupec, M. A.; Nazarov, A. A.; Severin, K.; Keppler, B. K. Transferring the Concept of Multinuclearity to Ruthenium Complexes for Improvement of Anticancer Activity. *J. Med. Chem.* **2009**, *52*, 916–925. (b) Loughrey, B. T.; Healy, P. C.; Parsons, P. G.; Williams, M. L. Selective Cytotoxic Ru(II) Arene Cp* Complex Salts $[R\text{-}PhRuCp^*]^+X^-$ for X = BF_4^-, PF_6^-, and BPh_4^-. *Inorg. Chem.* **2008**, *47*, 8589–8591. (c) Aird, R. E.; Cummings, J.; Ritchie, A. A.; Muir, M.; Morris, R. E.; Chen, H.; Sadler, P. J.; Jodrell, D. I. In Vitro and in Vivo Activity and Cross Resistance Profiles of Novel Ruthenium (II) Organometallic Arene Complexes in Human Ovarian Cancer. *Br. J. Cancer* **2002**, *86*, 1652–1657.

(4) (a) Tobe, M. L.; Burgess, J. *Inorganic Reaction Mechanisms*; Addison Wesley Longman Inc.: Essex, 1999. (b) Lay, P. A.; Harman, W. D. In *Advances in Inorganic Chemistry*; Sykes, A. G., Ed.; Academic Press: New York, 1991; Vol. 37, pp 219−379.

(5) (a) Helm, L.; Merbach, A. E. Water Exchange on Metal Ions: Experiments and Simulations. *Coord. Chem. Rev.* **1999**, *187*, 151–181. (b) Richens, D. T. Ligand Substitution Reactions at Inorganic Centers. *Chem. Rev.* **2005**, *105*, 1961–2002.

(6) (a) Cleare, M. J. Transition Metal Complexes in Cancer Chemotherapy. *Coord. Chem. Rev.* **1974**, *12*, 349–405. (b) Sava, G.; Giraldi, T.; Mestroni, G.; Zassinovich, G. Antitumor Effects of Rhodium-(I), Iridium(I) and Ruthenium(II) Complexes in Comparison with cis-dichlorodiammino Platinum(II) in Mice Bearing Lewis Lung Carcinoma. *Chem.-Biol. Interact.* **1983**, *45*, 1–6. (c) Sava, G.; Zorzet, S.; Perissin, L.; Mestroni, G.; Zassinovich, G.; Bontempi, A. Coordination Metal Complexes of Rh(I), Ir(I) and Ru(II): Recent Advances on Antimetastatic Activity on Solid Mouse Tumors. *Inorg. Chim. Acta* **1987**, *137*, 69–71. (d) Giraldi, T.; Sava, G.; Mestroni, G.; Zassinovich, G.; Stolfa, D. Antitumour Action of Rhodium(I) and Iridium(I) Complexes. *Chem.-Biol. Interact.* **1978**, *22*, 231–238. (e) Köpf-Maier, P. Complexes of Metals Other Than Platinum as Antitumour Agents. *Eur. J. Clin. Pharmacol.* **1994**, *47*, 1–16.

(7) (a) Casini, A.; Edafe, F.; Erlandsson, M.; Gonsalvi, L.; Ciancetta, A.; Re, N.; Ienco, A.; Messori, L.; Peruzzini, M.; Dyson, P. J. Rationalization of The Inhibition Activity of Structurally Related Organometallic Compounds Against the Drug Target Cathepsin B by DFT. *Dalton Trans.* **2010**, *39*, 5556–5563. (b) Amouri, H.; Moussa, J.; Renfrew, A. K.; Dyson, P. J.; Rager, M. N.; Chamoreau, L.-M. Discovery, Structure, and Anticancer Activity of an Iridium Complex of Diselenobenzoquinone. *Angew. Chem., Int. Ed. Engl.* **2010**, *49*, 7530–7533. (c) Ali Nazif, M.; Bangert, J.-A.; Ott, I.; Gust, R.; Stoll, R.; Sheldrick, W. S. Dinuclear Organoiridium(III) mono- and bis-intercalators with Rigid Bridging Ligands: Synthesis, Cytotoxicity and DNA Binding. *J. Inorg. Biochem.* **2009**, *103*, 1405–1414. (d) Wirth, S.; Rohbogner, C.; Cieslak, M.; Kazmierczak-Baranska, J.; Donevski, S.; Nawrot, B.; Lorenz, I.-P. Rhodium(III) and Iridium(III) Complexes with 1,2-naphthoquinone-1-oximate as a Bidentate Ligand: Synthesis, Structure, and Biological Activity. *J. Biol. Inorg. Chem.* **2010**, *15*, 429–440. (e) Gras, M.; Therrien, B.; Süss-Fink, G.; Casini, A.; Edafe, F.; Dyson, P. J. Anticancer Activity of New Organo-Ruthenium, Rhodium and Iridium Complexes Containing the 2-(pyridine-2-yl)thiazole N,N-chelating Ligand. *J. Organomet. Chem.* **2010**, *695*, 1119–1125. (f) Schäfer, S.; Sheldrick, W. S. Coligand Tuning of the DNA Binding Properties of Half-Sandwich Organometallic Intercalators: Influence of Polypyridyl (pp) and Monodentate Ligands (L = Cl, $(NH_2)_2CS$, $(NMe_2)_2CS$) on the Intercalation of (η^5-pentamethylcyclopentadienyl)-iridium(III)-dipyridoquinoxaline and -dipyridophenazine Complexes. *J. Organomet. Chem.* **2007**, *692*, 1300–1309. (g) Kokoschka, M.; Bangert, J. A.; Stoll, R.; Sheldrick, W. S. Sequence-Selective Organoiridium DNA bis-intercalators with Flexible Dithiaalkane Linker Chains. *Eur. J. Inorg. Chem.* **2010**, 1507–1515. (h) Hartinger, C. G. Trapping Unstable Benzoquinone Analogues by Coordination to a [(η^5-C_5Me_5)Ir] Fragment and the Anticancer Activity of the Resulting Complexes. *Angew. Chem., Int. Ed. Engl.* **2010**, *49*, 8304–8305. (i) Leung, S.-K.; Kwok, K. Y.; Zhang, K. Y.; Lo, K. K.-W. Design of Luminescent Biotinylation Reagents Derived from Cyclometalated Iridium(III) and Rhodium(III) Bis(pyridylbenzaldehyde) Complexes. *Inorg. Chem.* **2010**, *49*, 4984–4995. (j) Shao, F.; Barton, J. K. Long-Range Electron and Hole Transport through DNA with Tethered Cyclometalated Iridium(III) Complexes. *J. Am. Chem. Soc.* **2007**, *129*, 14733–14738. (k) Sliwinska, U.; Pruchnik, F. P.; Ulaszewski, S.; Latocha, M.; Nawrocka-Musial, D. Properties of η^5-pentamethylcyclopentadienyl Rhodium(III) and Iridium(III) Complexes with Quinolin-8-ol and Their Cytostatic Activity. *Polyhedron* **2010**, *29*, 1653–1659.

(8) Wilbuer, A.; Vlecken, D. H.; Schmitz, D. J.; Kräling, K.; Harms, K.; Bagowski, C. P.; Meggers, E. Iridium Complex with Antiangiogenic Properties. *Angew. Chem., Int. Ed. Engl.* **2010**, *49*, 3839–3842.

(9) Messori, L.; Marcon, G.; Orioli, P.; Fontani, M.; Zanello, P.; Bergamo, A.; Sava, G.; Mura, P. Molecular Structure, Solution Chemistry and Biological Properties of the Novel [ImH][trans-$IrCl_4$(Im)(DMSO)],

(I) and of the Orange Form of $[(DMSO)_2H][trans\text{-}IrCl_4(DMSO)_2]$, (II), Complexes. *J. Inorg. Biochem.* **2003**, *95*, 37–46.

(10) Marcon, G.; Casini, A.; Mura, P.; Messori, L.; Bergamo, A.; Orioli, P. Biological Properties of IRIM, the Iridium(III) Analogue of (Imidazolium (Bisimidazole) Tetrachlororuthenate) (ICR). *Metal-Based Drugs* **2000**, *7*, 195–200.

(11) (a) Peacock, A. F. A.; Habtemariam, A.; Moggach, S. A.; Prescimone, A.; Parsons, S.; Sadler, P. J. Chloro Half-Sandwich Osmium(II) Complexes: Influence of Chelated N,N-Ligands on Hydrolysis, Guanine Binding, and Cytotoxicity. *Inorg. Chem.* **2007**, *46*, 4049–4059. (b) Chen, H.; Parkinson, J. A.; Morris, R. E.; Sadler, P. J. Highly Selective Binding of Organometallic Ruthenium Ethylenediamine Complexes to Nucleic Acids: Novel Recognition Mechanisms. *J. Am. Chem. Soc.* **2003**, *125*, 173–186.

(12) (a) Liu, H.-K.; Berners-Price, S. J.; Wang, F.; Parkinson, J. A.; Xu, J.; Bella, J.; Sadler, P. J. Diversity in Guanine-Selective DNA Binding Modes for an Organometallic Ruthenium Arene Complex. *Angew. Chem., Int. Ed. Engl.* **2006**, *45*, 8153–8156. (b) Liu, H.-K.; Parkinson, J. A.; Bella, J.; Wang, F.; Sadler, P. J. Penetrative DNA Intercalation and G-base Selectivity of an Organometallic Tetrahydroanthracene Ru^{II} Anticancer Complex. *Chem. Sci.* **2010**, 258–270.

(13) Liu, S.; Rebros, M.; Stephens, G.; Marr, A. C. Adding Value to Renewables: A One Pot Process Combining Microbial Cells and Hydrogen Transfer Catalysis to Utilise Waste Glycerol from Biodiesel Production. *Chem. Commun.* **2009**, 2308–2310.

(14) (a) Hanasaka, F.; Fujita, K.-i.; Yamaguchi, R. Synthesis of New Iridium N-Heterocyclic Carbene Complexes Bearing a Functionalized Cp* Ligand and Their High Catalytic Activities in the Oppenauer-Type Oxidation of Alcohol. *Organometallics* **2006**, *25*, 4643–4647. (b) Ito, M.; Endo, Y.; Tejima, N.; Ikariya, T. Bifunctional Triflylamide-Tethered Cp′Rh and Cp′Ir Complexes: A New Entry for Asymmetric Hydrogenation Catalysts. *Organometallics* **2010**, *29*, 2397–2399. (c) Kohl, G.; Pritzkow, H.; Enders, M. Rhodium(III) and Iridium(III) Complexes with Quinolyl-Functionalized Cp Ligands: Synthesis and Catalytic Hydrogenation Activity. *Eur. J. Inorg. Chem.* **2008**, 4230–4235. (d) Pontes da Costa, A.; Viciano, M.; Sanaú, M.; Merino, S.; Tejeda, J.; Peris, E.; Royo, B. First Cp*-Functionalized N-Heterocyclic Carbene and Its Coordination to Iridium. Study of the Catalytic Properties. *Organometallics* **2008**, *27*, 1305–1309.

(15) Liu, Z.; Habtemariam, A.; Pizarro, A. M.; Fletcher, S.; Clarkson, G.; Sadler, P. J. *ISBOMC' 10, 5th International Symposium on Bioorganometallic Chemistry*; Ruhr-University: Bochum, Germany, 2010; p 32.

(16) The synthesis of the Cp^{xbiph} Ir^{III} complex containing ethylenediamine was unsuccessful, and so, this complex is not reported.

(17) Pizarro, A. M.; Habtemariam, A.; Sadler, P. J. In *Medicinal Organometallic Chemistry (Topics in Organometallic Chemistry)*, 1st ed.; Jaouen, G., Metzler-Nolte, N., Ed.; Springer-Verlag: Heidelberg, Germany, 2010; Vol. 32, pp 21−56.

(18) (a) Hohmann, H.; Hellquist, B.; Van Eldik, R. Kinetics and Mechanism of the Complex Formation Reactions of Diaqua(ethylenediamine)- and Diaqua(tetraethylethylenediamine)palladium(II) with the Purine Nucleosides Adenosine and Inosine. *Inorg. Chem.* **1992**, *31*, 345–351.(b) Martin, R. B. In *Cisplatin: Chemistry and Biochemistry of a Leading Anticancer Drug*; Lippert, B., Ed.; VHCA & Wiley-VCH: Zürich, Switzerland, 1999; pp 181−205.

(19) Jennerwein, M.; Andrews, P. A. Effect of Intracellular Chloride on the Cellular Pharmacodynamics of cis-diamminedichloroplatinum(II). *Drug Metab. Dispos.* **1995**, *23*, 178–184.

(20) Krezel, A.; Bal, W. A Formula for Correlating pKa Values Determined in D_2O and H_2O. *J. Inorg. Biochem.* **2004**, *98*, 161–166.

(21) (a) Zhang, C. X.; Lippard, S. J. New Metal Complexes as Potential Therapeutics. *Curr. Opin. Chem. Biol.* **2003**, *7*, 481–489. (b) Deubel, D. V.; Lau, J. K.-C. In Silico Evolution of Substrate Selectivity: Comparison of Organometallic Ruthenium Complexes with the Anticancer Drug Cisplatin. *Chem. Commun.* **2006**, 2451–2453.

(22) (a) Mendoza-Ferri, M.-G.; Hartinger, C. G.; Eichinger, R. E.; Stolyarova, N.; Severin, K.; Jakupec, M. A.; Nazarov, A. A.; Keppler, B. K. Influence of the Spacer Length on the in Vitro Anticancer Activity of Dinuclear Ruthenium-Arene Compounds. *Organometallics* **2008**, *27*, 2405–2407. (b) Gramatica, P.; Papa, E.; Luini, M.; Monti, E.; Gariboldi, M.; Ravera, M.; Gabano, E.; Gaviglio, L.; Osella, D. Antiproliferative Pt(IV) Complexes: Synthesis, Biological Activity, and Quantitative Structure−Activity Relationship Modeling. *J. Biol. Inorg. Chem.* **2010**, *15*, 1157–1169.

(23) (a) Loh, S. Y.; Mistry, P.; Kelland, L. R.; Abel, G.; Harrap, K. R. Reduced Drug Accumulation as a Major Mechanism of Acquired Resistance to Cisplatin in a Human Ovarian Carcinoma Cell line: Circumvention Studies Using Novel Platinum (II) and (IV) Ammine/amine Complexes. *Br. J. Cancer* **1992**, *66*, 1109–1115. (b) Oldfield, S. P.; Hall, M. D.; Platts, J. A. Calculation of Lipophilicity of a Large, Diverse Dataset of Anticancer Platinum Complexes and the Relation to Cellular Uptake. *J. Med. Chem.* **2007**, *50*, 5227–5237.

(24) (a) Jaouen, G., Ed.; *Bioorganometallics: Biomolecules, Labeling, Medicine*; Wiley-VCH: Weinheim, Germany, 2006. (b) Chen, H.; Parkinson, J. A.; Parsons, S.; Coxall, R. A.; Gould, R. O.; Sadler, P. J. Organometallic Ruthenium(II) Diamine Anticancer Complexes: Arene-Nucleobase Stacking and Stereospecific Hydrogen-Bonding in Guanine Adducts. *J. Am. Chem. Soc.* **2002**, *124*, 3064–3082. (c) Kostrhunova, H.; Florian, J.; Novakova, O.; Peacock, A. F. A.; Sadler, P. J.; Brabec, V. DNA Interactions of Monofunctional Organometallic Osmium(II) Antitumor Complexes in Cell-Free Media. *J. Med. Chem.* **2008**, *51*, 3635–3643.

(25) Novakova, O.; Chen, H.; Vrana, O.; Rodger, A.; Sadler, P. J.; Brabec, V. DNA Interactions of Monofunctional Organometallic Ruthenium(II) Antitumor Complexes in Cell-Free Media. *Biochemistry* **2003**, *42*, 11544–11554.

(26) Fernández, R.; Melchart, M.; Habtemariam, A.; Parsons, S.; Sadler, P. J. Use of Chelating Ligands to Tune the Reactive Site of Half-Sandwich Ruthenium(II)−Arene Anticancer Complexes. *Chem.—Eur. J.* **2004**, *10*, 5173–5179.

(27) (a) Habtemariam, A.; Melchart, M.; Fernández, R.; Parsons, S.; Oswald, I. D. H.; Parkin, A.; Fabbiani, F. P. A.; Davidson, J. E.; Dawson, A.; Aird, R. E.; Jodrell, D. I.; Sadler, P. J. Structure-Activity Relationships for Cytotoxic Ruthenium(II) Arene Complexes Containing N,N-, N,O-, and O,O-Chelating Ligands. *J. Med. Chem.* **2006**, *49*, 6858–6868. (b) The parallel for Pt is the incorporation of intercalating side arms into square-planar Pt^{II} complexes, for example, Sundquist, W. J.; Bancroft, D. P.; Lippard, S. J. Synthesis, Characterization, and Biological Activity of cis-diammineplatinum(II) Complexes of the DNA Intercalators 9-aminoacridine and Chloroquine. *J. Am. Chem. Soc.* **1990**, *112*, 1590–1596. Ma, Z.; Choudhury, J. R.; Wright, M. W.; Day, C. S.; Saluta, G.; Kucera, G. L.; Bierbach, U. A. A Non-Cross-Linking Platinum-Acridine Agent with Potent Activity in Non-Small-Cell Lung Cancer. *J. Med. Chem.* **2008**, *51*, 7574–7580. (c) Bugarcic, T.; Nováková, O.; Halámiková, A.; Zerzánková, L.; Vrána, O. i.; Kašpárková, J.; Habtemariam, A.; Parsons, S.; Sadler, P. J.; Brabec, V. Cytotoxicity, Cellular Uptake, and DNA Interactions of New Monodentate Ruthenium(II) Complexes Containing Terphenyl Arenes. *J. Med. Chem.* **2008**, *51*, 5310–5319.

(28) Cayemittes, S.; Poth, T.; Fernandez, M. J.; Lye, P. G.; Becker, M.; Elias, H.; Merbach, A. E. Mechanistic Investigation on the Water Substitution in the η^5-Organometallic Complexes $Cp^*Ir(H_2O)_3^{2+}$ and $Cp^*Rh(H_2O)_3^{2+}$. *Inorg. Chem.* **1999**, *38*, 4309–4316.

(29) (a) Dobereiner, G. E.; Crabtree, R. H. Dehydrogenation as a Substrate-Activating Strategy in Homogeneous Transition-Metal Catalysis. *Chem. Rev.* **2009**, *110*, 681–703.(b) Oro, L. A., Claver, C., Eds. *Iridium Complexes in Organic Synthesis*; Wiley-VCH Verlag GmbH & Co. KgaA: Weinheim, Germany, 2009.

(30) Schäfer, S.; Ott, I.; Gust, R.; Sheldrick, W. S. Influence of the Polypyridyl (pp) Ligand Size on the DNA Binding Properties, Cytotoxicity and Cellular Uptake of Organoruthenium(II) Complexes of the Type $[(\eta^6\text{-}C_6Me_6)Ru(L)(pp)]^{n+}$ [L = Cl, n = 1; L = $(NH_2)_2CS$, n = 2]. *Eur. J. Inorg. Chem.* **2007**, 3034–3046. They recently reported the inactivity of the phenanthroline complex **4** towards MCF-7 breast and HT-29 colon cancer cells; incorporation of strongly intercalating dipyridoquinoxaline and dipyridophenazine ligands gave rise to cytotoxic complexes. The intercalating dipyridyl ligands can lead to initial DNA recognition with the possibility of a switch to nucleobase binding:

Schäfer, S.; Sheldrick, W. S. Coligand Tuning of the DNA Binding Properties of Half-Sandwich Organometallic Intercalators: Influence of Polypyridyl (pp) and Monodentate Ligands (L = Cl, $(NH_2)_2CS$, $(NMe_2)_2CS$) on the Intercalation of (η^5-pentamethylcyclopentadienyl)-iridium(III)-dipyridoquinoxaline and -dipyridophenazine Complexes. *J. Organomet. Chem.* **2007**, *692*, 1300–1309. In contrast, in the present report, dual mode DNA base binding and intercalation is possible for complexes **5** and **6**.

(31) Churchill, M. R.; Julis, S. A. Crystal Structure and Molecular Geometry of Homogeneous Hydrogenation Catalyst $[(\eta^5\text{-}C_5Me_5)\text{-}IrCl]_2(\mu\text{-}H)(\mu\text{-}Cl)$ and of Its Precursor $[(\eta^5\text{-}C_5Me_5)IrCl]_2(\mu\text{-}Cl)_2$. A Direct Comparison of $Ir(\mu\text{-}H)(\mu\text{-}Cl)Ir$ and $Ir(\mu\text{-}Cl)_2Ir$ Bridging Systems. *Inorg. Chem.* **1977**, *16*, 1488–1494.

(32) Youinou, M.-T.; Ziessel, R. Synthesis and Molecular Structure of a New Family of Iridium(III) and Rhodium(III) Complexes: $[(\eta^5\text{-}Me_5C_5)Ir(LL)X]^+$ and $[(\eta^5\text{-}Me_5C_5)Rh(LL)Cl]^+$; LL = 2,2′-bipyridine or 1,10-phenanthroline; X = Cl or H. Single Crystal Structures of $[(\eta^5\text{-}Me_5C_5)Ir(bpy)Cl]Cl$ and $[(\eta^5\text{-}Me_5C_5)Rh(phen)Cl]ClO_4$. *J. Organomet. Chem.* **1989**, *363*, 197–208.

(33) Gorol, M.; Roesky, H. W.; Noltemeyer, M.; Schmidt, H.-G. (η^5-Pentamethylcyclopentadienyl)iridium(III) Complexes with η^2-N,O and η^2-P,S Ligands. *Eur. J. Inorg. Chem.* **2005**, 4840–4844.

(34) Scharwitz, M.; Schäfer, S.; Almsick, T. v.; Sheldrick, W. S. Chlorido(η^5-pentamethylcyclopentadienyl)(1,10-phenanthroline-κ^2N, N′)iridium(III) Trifluoromethanesulfonate. *Acta Crystallogr.* **2007**, *E63*, m1111–m1113.

(35) Koelle, U. Organometallic Aqua Ions of the Transition Metals. *Coord. Chem. Rev.* **1994**, *135*−*136*, 623–650.

(36) Bugarcic, T.; Habtemariam, A.; Stepankova, J.; Heringova, P.; Kasparkova, J.; Deeth, R. J.; Johnstone, R. D. L.; Prescimone, A.; Parkin, A.; Parsons, S.; Brabec, V.; Sadler, P. J. The Contrasting Chemistry and Cancer Cell Cytotoxicity of Bipyridine and Bipyridinediol Ruthenium(II) Arene Complexes. *Inorg. Chem.* **2008**, *47*, 11470–11486.

(37) Wang, F.; Habtemariam, A.; van der Geer, E. P. L.; Fernández, R.; Melchart, M.; Deeth, R. J.; Aird, R.; Guichard, S.; Fabbiani, F. P. A.; Lozano-Casal, P.; Oswald, I. D. H.; Jodrell, D. I.; Parsons, S.; Sadler, P. J. Controlling Ligand Substitution Reactions of Organometallic Complexes: Tuning Cancer Cell Cytotoxicity. *Proc. Natl. Acad. Sci. U.S.A.* **2005**, *102*, 18269–18274.

(38) (a) Peacock, A. F. A.; Habtemariam, A.; Fernández, R.; Walland, V.; Fabbiani, F. P. A.; Parsons, S.; Aird, R. E.; Jodrell, D. I.; Sadler, P. J. Tuning the Reactivity of Osmium(II) and Ruthenium(II) Arene Complexes under Physiological Conditions. *J. Am. Chem. Soc.* **2006**, *128*, 1739–1748. (b) Peacock, A. F. A.; Parsons, S.; Sadler, P. J. Tuning the Hydrolytic Aqueous Chemistry of Osmium Arene Complexes with N,O-Chelating Ligands to Achieve Cancer Cell Cytotoxicity. *J. Am. Chem. Soc.* **2007**, *129*, 3348–3357.

(39) Wang, F.; Chen, H.; Parsons, S.; Oswald, I. D. H.; Davidson, J. E.; Sadler, P. J. Kinetics of Aquation and Anation of Ruthenium(II) Arene Anticancer Complexes, Acidity and X-ray Structures of Aqua Adducts. *Chem.—Eur. J.* **2003**, *9*, 5810–5820.

(40) Wang, F.; Bella, J.; Parkinson, J. A.; Sadler, P. J. Competitive Reactions of a Ruthenium Arene Anticancer Complex with Histidine, Cytochrome c and an Oligonucleotide. *J. Biol. Inorg. Chem.* **2005**, *10*, 147–155.

(41) Wang, F.; Xu, J.; Habtemariam, A.; Bella, J.; Sadler, P. J. Competition between Glutathione and Guanine for a Ruthenium(II) Arene Anticancer Complex: Detection of a Sulfenato Intermediate. *J. Am. Chem. Soc.* **2005**, *127*, 17734–17743.

(42) Reedijk, J. Bioinorganic Chemistry Special Feature: New Clues for Platinum Antitumor Chemistry: Kinetically Controlled Metal Binding to DNA. *Proc. Natl. Acad. Sci. U.S.A.* **2003**, *100*, 3611–3616.

(43) Fukamachi, T.; Chiba, Y.; Wang, X.; Saito, H.; Tagawa, M.; Kobayashi, H. Tumor Specific Low pH Environments Enhance the Cytotoxicity of Lovastatin and Cantharidin. *Cancer Lett.* **2010**, *297*, 182–189.

(44) (a) Herebian, D.; Sheldrick, W. S. Synthesis and DNA Binding Properties of Bioorganometallic (η^5-pentamethylcyclopentadienyl)iridium(III) Complexes of the Type $[(\eta^5\text{-}C_5Me_5)Ir(Aa)(dppz)]^+$ (dppz = dipyrido[3,2-*a*:2′,3′-*c*]phenazine, *n* = 1−3), with S-coordinated Amino Acids (Aa) or Peptide. *J. Chem. Soc., Dalton Trans.* **2002**, 966–974. (b) Annen, P.; Schildberg, S.; Sheldrick, W. S. (η^5-Pentamethylcyclopentadienyl)iridium(III) Complexes of Purine Nucleobases and Nucleotides: A Comparison with (η^6-arene)ruthenium(II) and (η^5-pentamethylcyclopentadienyl)rhodium(III) Species. *Inorg. Chim. Acta* **2000**, *307*, 115–124. (c) Yamanari, K.; Ito, R.; Yamamoto, S.; Konno, T.; Fuyuhiro, A.; Kobayashi, M.; Arakawa, R. Diastereomeric Separations and Crystal Structures of Rhodium(III) and Iridium(III) Complexes Containing Adenosine and Related Nucleosides. *Dalton Trans.* **2003**, 380–386. (d) Yamanari, K.; Ito, R.; Yamamoto, S.; Konno, T.; Fuyuhiro, A.; Fujioka, K.; Arakawa, R. Cyclic Tetramers Composed of Rhodium(III), Iridium(III), or Ruthenium(II) Half-Sandwich and 6-Purinethiones. *Inorg. Chem.* **2002**, *41*, 6824–6830.

(45) van Rijt, S. H.; Peacock, A. F. A.; Johnstone, R. D. L.; Parsons, S.; Sadler, P. J. Organometallic Osmium(II) Arene Anticancer Complexes Containing Picolinate Derivatives. *Inorg. Chem.* **2009**, *48*, 1753–1762.

(46) van Rijt, S. H.; Mukherjee, A.; Pizarro, A. M.; Sadler, P. J. Cytotoxicity, Hydrophobicity, Uptake, and Distribution of Osmium(II) Anticancer Complexes in Ovarian Cancer Cells. *J. Med. Chem.* **2010**, *53*, 840–849.

(47) Jung, Y.; Lippard, S. J. Direct Cellular Responses to Platinum-Induced DNA Damage. *Chem. Rev.* **2007**, *107*, 1387–1407.

(48) In separate experiments, we have shown that complex **6** is significantly more active towards wild-type CHO-K1 cells as compared to its mutant cell line MMC-2, which carries an ERCC3/XPB mutation (ERCC3 is an ATP-dependent DNA helicase that plays an essential role in nucleotide excision repair). Thus, cells that are deficient in DNA repair are more sensitive to killing by complex **6**. This suggests that the cell must remove or bypass DNA lesions if it is to survive treatment and implies that unrepaired DNA damage contributes to its cytotoxicity. These data will be reported elsewhere.

(49) (a) Keck, M. V.; Lippard, S. J. Unwinding of Supercoiled DNA by Platinum-Ethidium and Related Complexes. *J. Am. Chem. Soc.* **1992**, *114*, 3386–3390. (b) Kasparkova, J.; Marini, V.; Najajreh, Y.; Gibson, D.; Brabec, V. DNA Binding Mode of the Cis and Trans Geometries of New Antitumor Nonclassical Platinum Complexes Containing Piperidine, Piperazine, or 4-Picoline Ligand in Cell-Free Media. Relations to Their Activity in Cancer Cell Lines. *Biochemistry* **2003**, *42*, 6321–6332.

(50) Satyanarayana, S.; Dabrowiak, J. C.; Chaires, J. B. Neither Δ- nor Λ-tris(phenanthroline)ruthenium(II) Binds to DNA by Classical Intercalation. *Biochemistry* **1992**, *31*, 9319–9324.

(51) Morris, R. E.; Aird, R. E.; del Socorro Murdoch, P.; Chen, H.; Cummings, J.; Hughes, N. D.; Parsons, S.; Parkin, A.; Boyd, G.; Jodrell, D. I.; Sadler, P. J. Inhibition of Cancer Cell Growth by Ruthenium(II) Arene Complexes. *J. Med. Chem.* **2001**, *44*, 3616–3621.

(52) (a) Barry, N. P. E.; Edafe, F.; Dyson, P. J.; Therrien, B. Anticancer Activity of Osmium Metalla-Rectangles. *Dalton Trans* **2010**, *39*, 2816–2820. (b) Peacock, A. F. A.; Sadler, P. J. Medicinal Organometallic Chemistry: Designing Metal Arene Complexes as Anticancer Agents. *Chem. Asian J.* **2008**, *3*, 1890–1899.

(53) (a) Allen, O. R.; Gott, A. L.; Hartley, J. A.; Hartley, J. M.; Knox, R. J.; McGowan, P. C. Functionalised Cyclopentadienyl Titanium Compounds as Potential Anticancer Drugs. *Dalton Trans.* **2007**, 5082–5090. (b) Tan, Y. L. K.; Pigeon, P.; Hillard, E. A.; Top, S.; Plamont, M.-A.; Vessieres, A.; McGlinchey, M. J.; Muller-Bunz, H.; Jaouen, G. Synthesis, Oxidation Chemistry and Cytotoxicity Studies on Ferrocene Derivatives of Diethylstilbestrol. *Dalton Trans.* **2009**, 10871–10881.

(54) *CrysAlis PRO*; Oxford Diffraction Ltd.: Abington, Oxfordshire, United Kingdom, 2007.

(55) Sheldrick, G. M. Phase Annealing in SHELX-90: Direct Methods for Larger Structures. *Acta Crystallogr.* **1990**, *A46*, 467–473.

(56) Sheldrick, G. M. *SHELXL-97*; University of Göttingen: Göttingen, Germany, 1997.

(57) Frisch, M. J.; Trucks, G. W.; Schlegel, H. B.; Scuseria, G. E.; Robb, M. A.; Cheeseman, J. R.; Montgomery, J. A., Jr.; Vreven, T.; Kudin, K. N.; Burant, J. C.; Millam, J. M.; Iyengar, S. S.; Tomasi, J.; Barone, V.; Mennucci, B.; Cossi, M.; Scalmani, G.; Rega, N.; Petersson, G. A.; Nakatsuji, H.; Hada, M.; Ehara, M.; Toyota, K.; Fukuda, R.;

Hasegawa, J.; Ishida, M.; Nakajima, T.; Honda, Y.; Kitao, O.; Nakai, H.; Klene, M.; Li, X.; Knox, J. E.; Hratchian, H. P.; Cross, J. B.; Bakken, V.; Adamo, C.; Jaramillo, J.; Gomperts, R.; Stratmann, R. E.; Yazyev, O.; Austin, A. J.; Cammi, R.; Pomelli, C.; Ochterski, J. W.; Ayala, P. Y.; Morokuma, K.; Voth, G. A.; Salvador, P.; Dannenberg, J. J.; Zakrzewski, V. G.; Dapprich, S.; Daniels, A. D.; Strain, M. C.; Farkas, O.; Malick, D. K.; Rabuck, A. D.; Raghavachari, K.; Foresman, J. B.; Ortiz, J. V.; Cui, Q.; Baboul, A. G.; Clifford, S.; Cioslowski, J.; Stefanov, B. B.; Liu, G.; Liashenko, A.; Piskorz, P.; Komaromi, I.; Martin, R. L.; Fox, D. J.; Keith, T.; Al-Laham, M. A.; Peng, C. Y.; Nanayakkara, A.; Challacombe, M.; Gill, P. M. W.; Johnson, B.; Chen, W.; Wong, M. W.; Gonzalez, C.; Pople, J. A. *Gaussian 03*, revision D.01; Gaussian, Inc.: Wallingford, CT, 2003.

(58) Adamo, C.; Barone, V. Toward Reliable Density Functional Methods without Adjustable Parameters: The PBE0Model. *J. Chem. Phys.* **1999**, *110*, 6158–6170.

(59) Hay, P. J.; Wadt, W. R. Ab Initio Effective Core Potentials For Molecular Calculations. Potentials for the Transition Metal Atoms Sc to Hg. *J. Chem. Phys.* **1985**, *82*, 270–283.

(60) McLean, A. D.; Chandler, G. S. Contracted Gaussian Basis Sets for Molecular Calculations. I. Second Row Atoms, Z = 11−18. *J. Chem. Phys.* **1980**, *72*, 5639–5648.

(61) Skehan, P.; Storeng, R.; Scudiero, D.; Monks, A.; McMahon, J.; Vistica, D.; Warren, J. T.; Bokesch, H.; Kenney, S.; Boyd, M. R. New Colorimetric Cytotoxicity Assay for Anticancer-Drug Screening. *J. Natl. Cancer Inst.* **1990**, *82*, 1107–1112.

(62) Novakova, O.; Kasparkova, J.; Vrana, O.; van Vliet, P. M.; Reedijk, J.; Brabec, V. Correlation between Cytotoxicity and DNA Binding of Polypyridyl Ruthenium Complexes. *Biochemistry* **1995**, *34*, 12369–12378.

(63) (a) Butour, J.-L.; Macquet, J.-P. Differentiation of DNA · Platinum Complexes by Fluorescence. *Eur. J. Biochem.* **1977**, *78*, 455–463. (b) Butour, J.-L.; Alvinerie, P.; Souchard, J.-P.; Colson, P.; Houssier, C.; Johnson, N. P. Effect of the Amine Non-Leaving Group on the Structure and Stability of DNA Complexes with cis-[Pt(R-$NH_2)_2(NO_3)_2$]. *Eur. J. Biochem.* **1991**, *202*, 975–980.